# Inorganic Nanoparticles Change Cancer Cell-Derived Extracellular Vesicle Secretion Levels and Cargo Composition Resulting in Secondary Biological Effects

*Kiana Buttiens[1], Christy Maksoudian[1], Irati Perez Gilabert[1], Carla Rios Luci[1], Bella B. Manshian[2,3], Stefaan J. Soenen[1,3]**

1. NanoHealth and Optical Imaging Group, Department of Imaging and Pathology, KU Leuven, Herestraat 49, B3000 Leuven, Belgium - 2. Translational Cell and Tissue Research Unit, Department of Imaging and Pathology, KU Leuven, Herestraat 49, B3000 Leuven, Belgium - 3. Leuven Cancer Institute, KU Leuven, Herestraat 49, B3000 Leuven, Belgium

*Corresponding author: s.soenen@kuleuven.be

KEYWORDS: nanoparticles, extracellular vesicles, cancer, exosomal miRNA, toxicity

***Manuscript published in ACS Applied Materials & Interfaces, 2024, 16, 66-83.***

**Abstract**

Over the past decades, the medical exploitation of nanotechnology has been largely increasing and finding its way into translational research and clinical applications. Despite their biomedical potential, uncertainties persist regarding the intricate role that nanomaterials may play on altering physiology in healthy and diseased tissues. Extracellular vesicles (EVs) are recognized as an important pathway for intercellular communication and known to be mediators of cellular stress. EVs are currently explored for targeted delivery of therapeutic agents, including nanoformulations, to treat and diagnose cancer or other diseases. Here, we aimed to investigate whether nanomaterials could have a possible impact on EV functionality, their safety and whether EVs can play a role in nanomaterial toxicity profiles. To evaluate this, the impact of inorganic nanomaterial administration on EVs derived from murine melanoma and human breast cancer cells was tested. Cells were incubated with subtoxic concentrations of 4 different biomedically relevant inorganic nanoparticles (NPs): gold, silver, silicon dioxide or iron oxide. The results displayed a clear NP and cell-type dependent effect on increasing or decreasing EV secretion. Furthermore, the expression pattern of several EV-derived miRNAs was significantly changed upon NP exposure, compared to non-treated cells. Detailed pathway analysis and additional studies confirmed that EVs obtained from NP-exposed cells could influence immunological responses and cellular physiology. Together, these data reveal that NPs can have wide-ranging effects which can result in toxicity concerns or enhanced therapeutic potential as a secondary enhanced effect mediated and enhanced by EVs.

## Introduction

The biomedical use of inorganic nanoparticles (NPs) is a major research focus, in particular in view of tumor diagnostics or therapy.[1] Not only for their use as targeted carriers of therapeutic formulations, but also for their intrinsic anti-tumor properties they have received considerable attention over the past decades.[2–4] More specifically, inorganic nanomaterials have been highlighted for their capacity to suppress tumor cell migration in preclinical studies [5,6]. Beside their use as drug carriers or for their intrinsic drug properties, inorganic nanomaterials can also be applied as guiding probes for diagnostic or -combined- theragnostic purposes [7]. This has all lead to substantial interest in the use of inorganic nanomaterials for (targeted) delivery at tumor sites.

Despite the wide range of promising preclinical results, one of the shortcomings lies in the relatively low delivery of NPs to the specific tumor site [8]. For a long time, it was believed that inorganic NPs are able to passively diffuse towards the tumor site by means of the enhanced permeability and retention effect, but recent studies have called these findings into question [9]. Various strategies have been employed to increase the delivery of NPs to solid tumors,[10] but thus far, the efficacy remains fairly low. One possible approach is the loading of NPs into extracellular vesicles (EVs).[11,12] These are membrane bound vesicles, enclosed with a lipid bilayer and secreted by all kinds of eukaryotic and prokaryotic cells.[13] EVs by itself function as an important mediator of intercellular communication, as they deliver their specific cargo (such as proteins, nucleic acids and other metabolites) to receptor cells locally (for example, within the tumor microenvironment) or at distant locations (for example, at metastatic sites).[14,15] EVs are classified based on their type of biogenesis and/or size into three larger groups: exosomes (<150 nm), microvesicles (150-1000 nm) and apoptotic bodies (>1000 nm).[13]

The field of EVs has also known growing interest over the past decades, including but not only for their potential use in nanomedicine. Interestingly, EVs were found to play an essential role in metastatic processes by their contribution to the formation of a so-called "pre-metastatic niche" environment.[16] As they are nanosized vesicles of endogenous origin, EVs entail several advantages such as their low toxicity, high stability and uncomplicated crossing of biological barriers. In view of these characteristics, they are often applied in targeting strategies for nanoformulations.[11] They are also often used for specific delivery of encapsulated cargo, such as drugs or small RNA sequences.[17] Additionally, EVs can play a major role in the characterization of aberrant physiology, where specific EV profiles can be a marker for tumor growth or can indicate the degree of malignancy or response to cancer therapy.[18] EVs are therefore seen as a powerful biomedical agent that can help to transform the (pre)clinical landscape in the near future by enabling personalized strategies. However, great care must be taken with regard to the safe use of EVs, as their lipid composition, and the genetic cargo they contain upon generation can influence cell behavior, and could have profound effects. This was illustrated by the work by Zomer *et al.*,[19] who found that EVs derived from malignant tumors were able to increase the level of malignancy in more benign tumors and thus increase metastases levels.

In current research strategies, inorganic NPs are often used in the context of EVs, such as the targeted delivery of inorganic NPs. Furthermore, gold NPs are currently being investigated as nanotheragnostics for both EV quantification and the 'therapeutic' targeting of (malicious) EVs.[20] Various NPs have also been used to improve the generation and purification of EVs,[21] and EVs have been involved in the intercellular transfer of NPs.[22]

The increased combination of inorganic NPs and EVs begs the question to what extent the use of these NPs may influence the EVs that have been generated, and in

doing so, whether this could hold advantages or disadvantages concerning the functional use of these EVs. Questions regarding the safety of inorganic NPs are still persisting, and a wide range of effects have also been described at sub-cytotoxic concentrations, including alterations in signaling pathways and gene expression.[23,24] Many studies have furthermore demonstrated clear biomedical effects of inorganic NPs on solid tumors, such as the generation of an anti-tumor immune response driven by iron oxide NPs (IONPs)-mediated polarization of tumor-associated macrophages, or a decrease or increase of metastasis by Au NPs, driven by cancer associated fibroblast signaling pathways, or the generation of endothelial gaps, respectively.[5,25] As multiple studies have shown that only a very low number of cells in the tumor microenvironment will interact with intravenously administered NPs, the extent of some of these effects remains a bit puzzling. We therefore hypothesize that these effects are not necessarily directly caused by the NPs themselves, but the initial effects may be enhanced by the cellular secretome, of which the EVs make up an important component. The potential of IONP-induced EVs generation has already been described, where pulmonary exposure to iron oxide particles was found to generate a dose-dependent release of EVs, which in turn resulted in systemic immune activation.[26]

In regard of all of the abovementioned factors, we consider it highly valuable to further elucidate how inorganic NPs may potentially alter the characteristics of (cancer) cell-derived EVs in a quantitative and qualitative manner, for this will be essential to safeguard their further translation towards the clinic.

In this study we have therefore investigated the impact of four different biomedically relevant inorganic nanoparticles: Gold (Au NPs), Silver (Ag NPs), Silicon dioxide ($SiO_2$) (Si NPs) and iron oxide (IONP) on the generation of EVs, their genetic cargo, and the potential implications thereof.

## Results and Discussion

### Nanoparticle characterization

In our study, 4 different biomedically relevant inorganic nanoparticles were used, being Au, Ag, $SiO_2$, and IONPs with core sizes of 20 nm, 4 nm, 30 nm and 4 nm respectively.

NP core sizes were determined by transmission electron microscopy (TEM). Hydrodynamic size and polydispersity index (PDI) were measured by dynamic light scattering (DLS), and confirmed by nanoparticle tracking analysis (NTA). The surface charge (ζ-potential) was measured using a zetasizer system. An overview of NP characterization results can be found in **Figure 1**.

TEM analysis confirmed the core size of the NPs to be highly similar to the values provided by the distributor of the NPs. Due to presence of polymeric (poly(metacrylic acid); PMA) surface coatings on most of the NPs, hydrodynamic sizes were on average approximately 15 nm larger than core size, as was expected. For $SiO_2$, this increase was missing, which is due to the fact that the $SiO_2$ NPs were not coated by PMA, but instead contained silanol end groups, which provided the overall negative charge and colloidal stability. Overall, the PdI was relatively low, in particular for such small NPs, yet this was not so for the IONPs, although the precise reason for it remained unclear. The low PdI values highlight the relatively high degree of monodisperse NPs, as has been detailed elsewhere.[27,28] No aggregation was ever observed by the naked eye, and the TEM analysis also did not indicate any broad distribution in core sizes of the NPs. The colloidal stability of the NPs was then analyzed in serum-containing medium using NTA, revealing a very similar size as obtained by DLS in the absence of serum. These data indicate that the NPs seem quite stable in the presence of serum. Overall, these 4 NPs were chosen as model

systems to study their effects on the secretome of incubated cells, and specifically the EV compartment. For that purpose, we chose NPs with different properties, where all 4 had different cores compositions, 2 of them are 4nm core diameter, one was 20 nm diameter and one was 30 nm diameter; while 2 of them are coated with PMA (Ag, IONP), while the Au NPs are coated with poly (acryclic acid) (PAA) polymer). While the similarities between some NPs would allow us to compare whether one property may play a vital role in affecting the EVs, we mainly wanted to ensure that a large group of NPs is included such that any effects we may observe cannot be solely ascribed to a particular size, chemical composition or surface chemistry.

**A)**

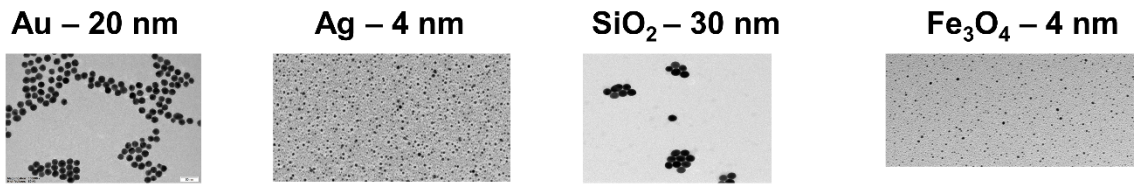


**B)**

| NP | 1. TEM (nm) | 2. DLS (nm) | 3. PDI | 4. ζ-pot (mV) | 5. NTA (nm) |
|---|---|---|---|---|---|
| **Au** | 19.2 ± 2.1 | 34.9 ± 2.9 | 0.229 | - 49.4 ± 5.2 | 27 ± 1.7 |
| **Ag** | 5.2 ± 1.8 | 19.1 ± 2.4 | 0.274 | -61.2 ± 6.1 | 21 ± 3.1 |
| **$SiO_2$** | 31.3 ± 3.4 | 43.4 ± 3.2 | 0.228 | -67.9 ± 4.7 | 42 ± 3.8 |
| **$Fe_3O_4$** | 4.7 ± 2.2 | 23.4 ± 3.5 | 0.224 | -63.3 ± 5.3 | 29 ± 2.7 |

**Figure 1. Nanoparticle characterization**. **A)** Representative transmission electron microscopy pictures for the different NPs used in this study. Scale bar used is 50 nm. **B)** Different parameters assessed for all NPs used in this study: 1. Transmission electron microscopy (TEM), measuring Core particle diameter (in nm) of 100 NPs over different images of each sample. 2. Hydrodynamic diameter (in nm) in aqueous environment measured in PBS with dynamic light scattering (DLS). 3. Polydispersity index (PDI) by DLS indicates colloidal stability of the NPs in PBS. 4. ζ-potential represents the NP surface charge (in mV), measured in PBS. 5. Nanoparticle tracking analysis (NTA) measures colloidal stability, concentration and size distribution of the NPs (in nm). Data is represented as mean ± SD for 3 independent repeats, with n= 3 for all methods, apart from NTA (n = 5).

**Cell-Nanoparticle interaction studies - in vitro high-content analysis**

To study cellular secretome effects in view of tumor physiology, two commonly used cancer cell lines have been selected. One is a B16F10 murine melanoma cell line, while the other is a human triple negative breast cancer cell line (MDA-MB-231). Both cell types have been widely used in cancer research, as well as in NP toxicity studies and EV characterization.[29,30] To explore the effect of inorganic nanomaterials on EV concentrations and their contents, it is important to select NP concentrations that do not compromise cell growth (number) or cell viability in general and, as such, are not toxic to the cells. We therefore evaluated cell viability in both the MDA-MB-231 and B16F10 cells that were exposed for 24 hours to a range of concentrations for each of the NPs of interest to determine their cell-specific subtoxic range. We then evaluated cellular wellbeing using an established high-content imaging setup, measuring cell viability and mitochondrial ROS.[31]

The lowest concentrations at which significant toxicity was observed in the cytotoxicity assay using MDA-MB-231 cells were 8 nM (Ag), 200 µg/mL ($SiO_2$) and 80 nM (IONP) in MDA-MB-231 cells (**Figure 2**). Gold NPs do not exert any cytotoxic effects in MDA-MB-231 cells up to concentrations of 5 nM. For B16F10 cells significant cytotoxicity was observed from 100 µg/mL ($SiO_2$) and 250 nM (IONP). Gold and silver NPs do not exert any significant cytotoxic effect in B16-F10 cells up to concentrations of 5 and 10 nM respectively. Apart from $SiO_2$ NPs, no effects were noticed on mitochondrial reactive oxygen species (ROS) formation on the cells under the conditions used, suggesting that under these conditions, mitochondrial ROS did not play a significant role in NP toxicity (**Supporting Figure S1**). Overall, under the conditions tested, Au NPs appeared to exert the least toxicity, while Ag, IONPs and $SiO_2$ NPs all demonstrated concentration-dependent toxicity. For Ag and IONPs, this

is in line with expectations, as upon cellular internalization, and exposure to a more acidic endolysosomal environment, these NPs can start to degrade and release high local metal ion concentrations that can exceed toxic thresholds.

For our follow-up studies, we selected a range of concentrations to determine EV generation levels up to 6 nM as the maximal concentration for Au and Ag NPs, 30

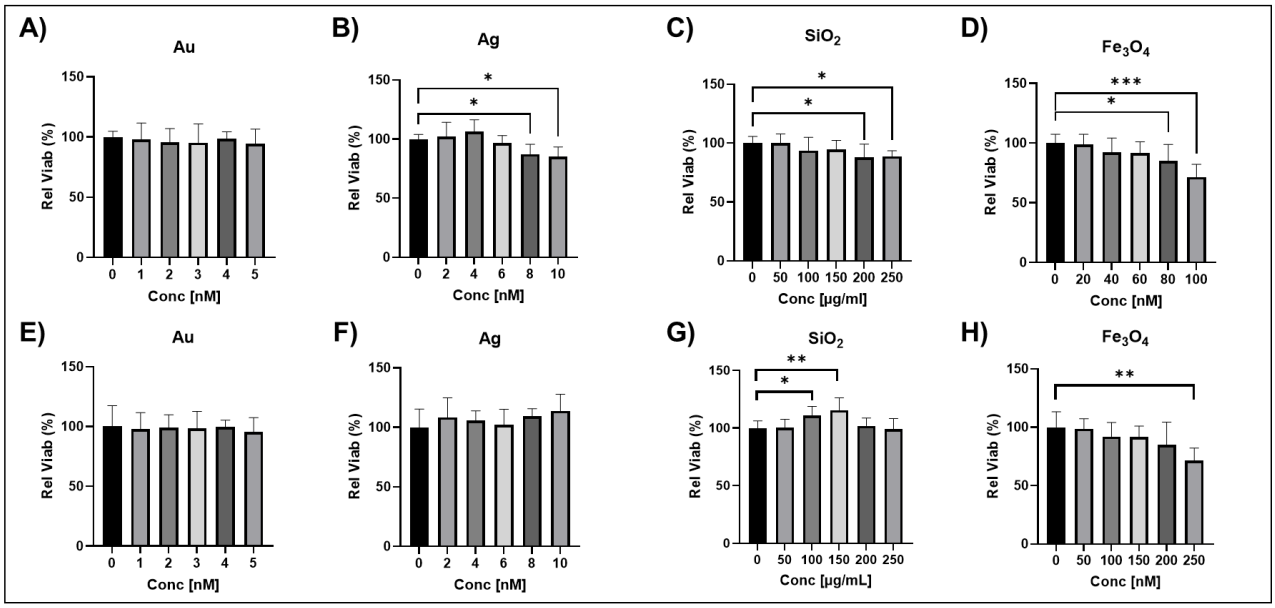


µg/ml for $SiO_2$ NPs and 30 nM

***Figure 2. Nano-bio interaction studies: Cell viability.*** *(n=5) In vitro high content analysis results for cell viability are shown: for MDA-MB-231 cells incubated for 24 hrs with* ***A)*** *Gold (20 nm, polymer coated)* ***B)*** *Silver (4 nm, PMA coated)* ***C)*** *Silicon oxide (30 nm, COOH coated)* ***D)*** *Iron oxide (4 nm, PMA coated). *p<0.05, **p<0.005, ***p<0.0005 vs negative control (0 nM). For B16-F10 cells incubated for 24 hrs with* ***E)*** *Gold (20 nm, polymer coated)* ***F)*** *Silver (4 nm, PMA coated)* ***G)*** *Silicon oxide (30 nm, COOH coated)* ***H)*** *Iron oxide (4 nm, PMA coated). *p<0.05, **p<0.005, ***p<0.0005 vs negative control (0 nM). Data is represented as mean ± SD.*

for IONPs. These concentrations were selected as concentrations where no direct cytotoxicity was induced by the NPs themselves in either of the two cell types and

the generation of EVs would therefore be more easy to analyze than in conditions with elevated cell death where apoptotic bodies or membrane fragments could hamper EV analysis.

**Isolation and Characterization of Extracellular vesicles from cell culture supernatant**

Further studies are performed on extracellular vesicles isolated from concentrated conditioned cell culture medium (CCM) of MDA-MB-231 or B16F10 cells that underwent different nanoparticle treatments, by following the steps as shown in **Figure 3**. To standardize for the applied isolation protocol, the quality and quantity of eluted vesicles are determined by a range of different methods in accordance with the Minimal Informative Studies of Extracellular Vesicles (MISEV) 2018 guidelines[32]: TEM images from a representative sample show that isolated EVs are typically cup-shaped and delineated by a lipid bilayer. Administration of inorganic nanoparticles to the cells does not affect these parameters in cell supernatant-derived EVs, as shown in **Figure 4a**. To confirm whether the vesicular structures are indeed secreted vesicles and not cellular debris or apoptotic bodies generated by dying cells, Western Blotting of EV and cellular markers was performed (**Figure 4b**). EV-resident markers such as tumor susceptibility gene 101 (TSG101), were detected in isolated EV samples, while Calnexin, an intracellular component linked to the endoplasmic reticulum (ER), used here as negative control, is not detected in the isolated EV sample.[32] The latter confirms the absence of contamination from cellular components in the isolated EV sample and the high purity thereof, indicating furthermore the absence of (Calnexin+) apoptotic bodies. The data reveal the clear presence of TSG101 in both cells as well as isolated vesicles, indicating that the observed structures are indeed cell-derived. Importantly, while cells also contain the endoplasmic reticulum marker Calnexin, this marker was completely absent from the isolated vesicles. Furthermore, NTA was performed to determine the hydrodynamic size and concentration of the isolated EVs (**Figure 4c**). The majority of isolated EVs are in the size range of 50 to 300 nm, which is indicative of the general size range of EVs, which generally, can be split into smaller exosomes (50-150 nm) and somewhat larger microvesicles (up to 1 µm), while

they can also contain apoptotic bodies. Multiple peaks detected in hydrodynamic size analysis are a possible consequence of the heterogeneity of the purified EV sample. Results from TEM and NTA analysis are all in line with the expected size and morphology of EVs.

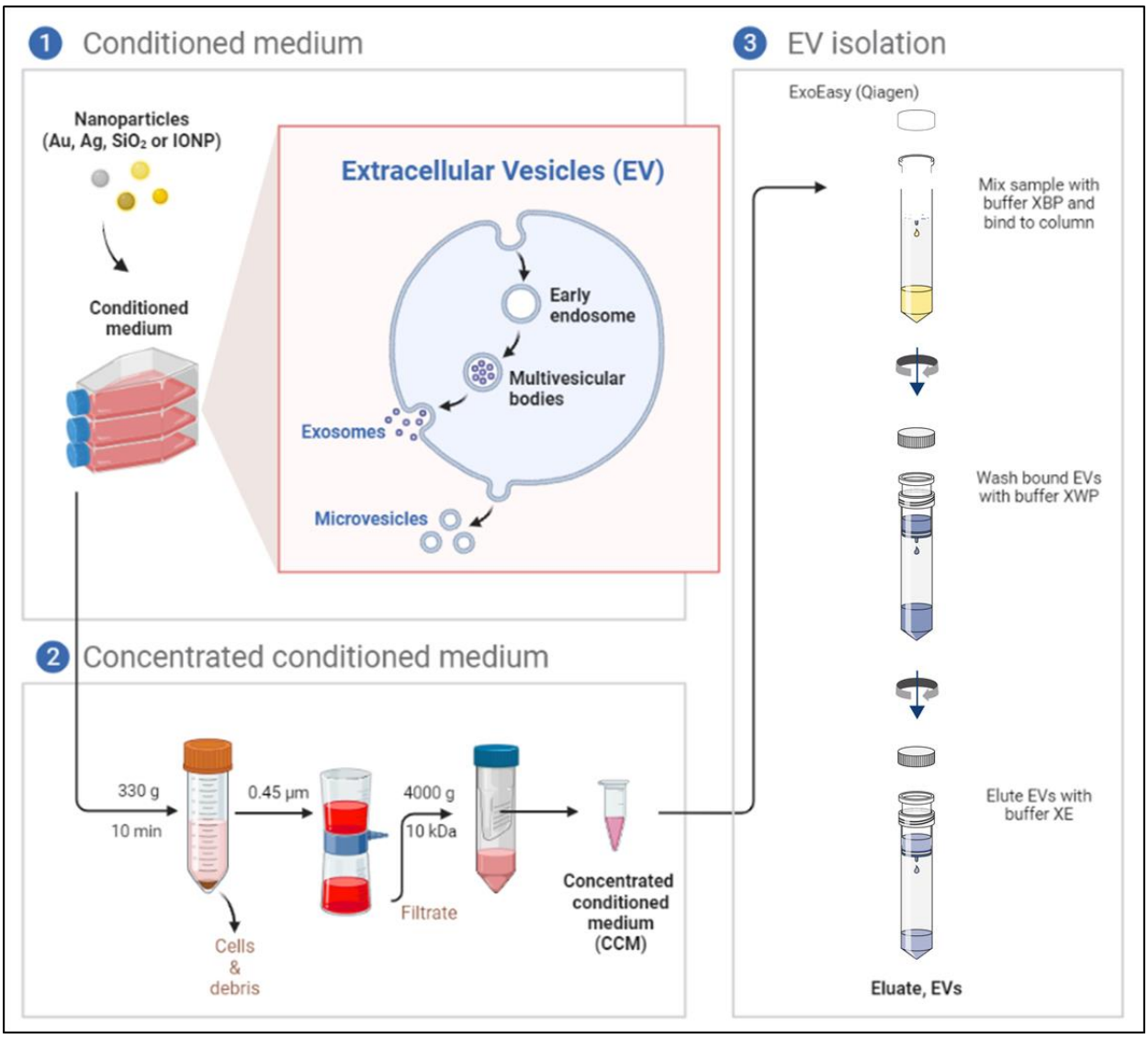


***Figure 3. Extracellular vesicle isolation.*** *Workflow for the isolation of extracellular vesicles (EVs) from concentrated conditioned medium (CCM). The protocol is completed at 4°C. EVs are stored at -80°C for further downstream analysis. Figure created with Biorender.com*

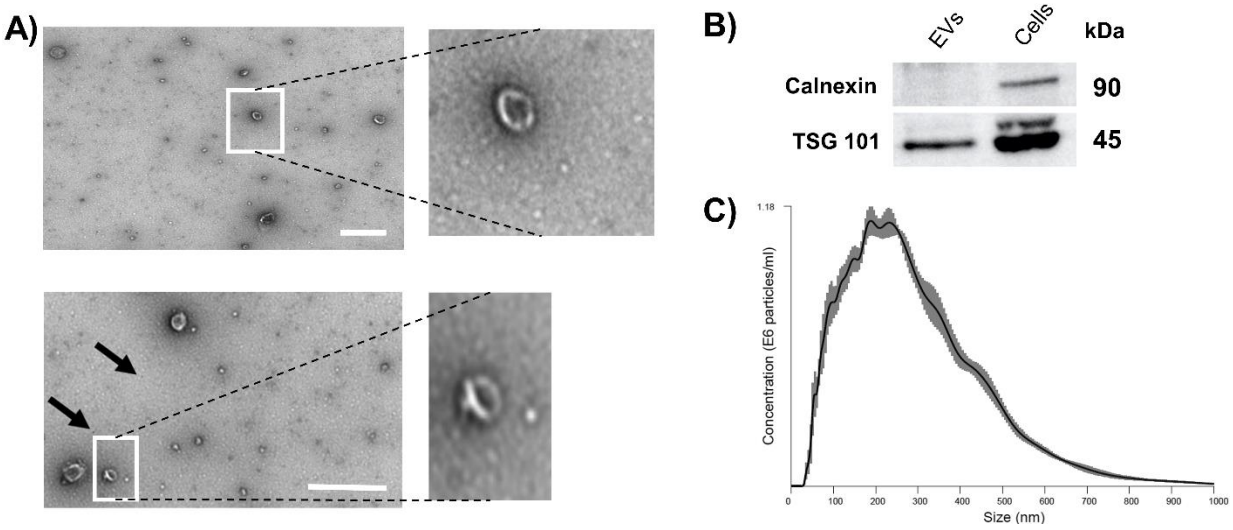


***Figure 4. Extracellular vesicle characterization.*** *Extracellular vesicles isolated and analyzed in this study are first characterized for size, shape, concentration and protein content by:* ***A)*** *TEM of EVs isolated from MDA-MB-231 cell culture supernatant. Scale bar used is 1 µm. Black arrows indicate NP presence.* ***B)*** *Western blot of EV- and cell lysates, confirming presence of EV marker (TSG101) and absence of negative control Calnexin (ER-marker) in EV lysates derived from MDA-MB-231 cells* ***C)*** *Nanoparticle tracking analysis (NTA) of purified EV samples displaying the averaged (n=5) size distribution/concentration of EVs isolated from MDA-MB-231 cell culture supernatant. Grey error bars indicate +/- 1 standard error of the mean.*

### *Quantitative EV analysis using image-based flow cytometry*

After several washing rounds of seeded cells with serum-free medium, cells are treated with a subtoxic range of each of the 4 inorganic nanomaterials (gold, silver, silicon dioxide, iron oxide) for 24 hrs, after which the medium is removed, cells are extensively washed to remove any remnant NPs and the cells are then left to incubate with medium containing EV-depleted FBS for an additional 24 hrs. The conditioned cell supernatant including cell-derived EVs is then collected and EVs are purified by a membrane-based affinity binding kit. Freshly isolated EVs are then double-labeled fluorescently for EV-specific markers, being the tetraspanin CD63[33] and Alix, involved in exosome biogenesis[34], and quantified by image-based flow cytometry (**Figure 5a**). Image-based flow cytometry has been frequently described as an excellent tool for

quantitative analysis of EVs, unlike normal flow cytometry where the small size of the EVs may impede analysis.[35] Here, the system contains small speedbeads, which are fluorescently labeled with a far red dye and specific gating strategies were set up to identify $CD63^+$ $Alix^+$ EVs that do not display any signal in the far red (speedbead) channel (**Figure 5b**). For Au and Ag NPs, a significant increase ($p<0.05$) in released EVs from MDA-MB-231 cells is detected at subcytotoxic concentrations of 2 and 4 nM respectively, compared to the control sample (0 nM). Potential effects of the NPs on cell viability could explain the non-significant (decreasing) trend from 6 nM onwards (**Figure 5c-f**). For IONPs, a sudden drop in EV generation occurred at higher concentrations, while for $SiO_2$, a clear concentration-dependent inhibition of EV secretion is observed. As the NPs are unlikely to interact with the readout itself, and the NPs were carefully washed away prior to EV removal, it is therefore possible that the presence of the NPs, and in particular the $SiO_2$ may affect EV generation or secretion. Based on their biogenesis, two major types of EVs can be distinguished, where exosomes are of endosomal origin, released upon the fusion of the limiting membrane of multivesicular bodies or amphisomes with the plasma membrane. EVs can on the other hand also be generated through the release of plasma membrane-derived EVs (so-called ectosomes, including apoptotic bodies or microvesicles).[36] EV synthesis can be influenced by a wide range of factors, including hypoxia, nutrient levels, viral egress, secretory autophagy, the cellular senescence-associated secretory phenotype or the DNA damage response.[37,38] At current, it remains unclear how $SiO_2$ NPs could reduce the number of EVs being generated. Thus far, EV secretion has been found to be reduced by agents such as simvastatin, by reducing cholesterol levels important in EV biogenesis.[39] While $SiO_2$ NPs have not been directly linked with inhibition of cholesterol synthesis, $SiO_2$ NPs have been described to reduce membrane fluidity.[40] This reduced fluidity may have a similar impact as the reduction in cholesterol and may affect EV biogenesis. An in-depth mechanistic investigation

of this finding is, however, outside of the scope of this study. For Au and Ag NPs administered to MDA-MB-231 cells, the increase in EV generation is in line with literature reports, where various different types of NPs have been associated with elevated EV levels.[41] The latter has mainly been ascribed to the induction of cellular (oxidative) stress, where any stressful conditions for the cells, such as lack of serum or hypoxia have been shown to promote EV biogenesis.[42] Interestingly, for B16F10, all NPs displayed a clear concentration-dependent decrease in EV secretion levels compared to untreated control cells (**Figure 5g-j**). As the NPs were all provided at subcytotoxic conditions, this result is somewhat strange and indicates that the effects of the NPs on EV-mediated secretion levels is highly cell type-dependent and thus cannot be generalized.

***Figure 5. Quantification of EV concentrations upon NP administration.*** *Relative EV concentrations from cell culture supernatant were determined by image-based flow cytometry upon 48 hr incubation with a range of subtoxic nanoparticle concentrations. A) Amnis Image stream software (IDEAS) analysis displaying double positive-labeled objects for EV markers CD63 and Alix. B) Example of gating strategies applied to distinguish EVs from speed beads and larger vesicles present in the fluidics system upon loading of an EV sample. Image based flow cytometry analysis results are shown for C,G) Gold (20 nm, polymer coated) D,H) Silver (4 nm, PMA coated) E,I) Silicon dioxide (30 nm, COOH coated) F,J) Iron*

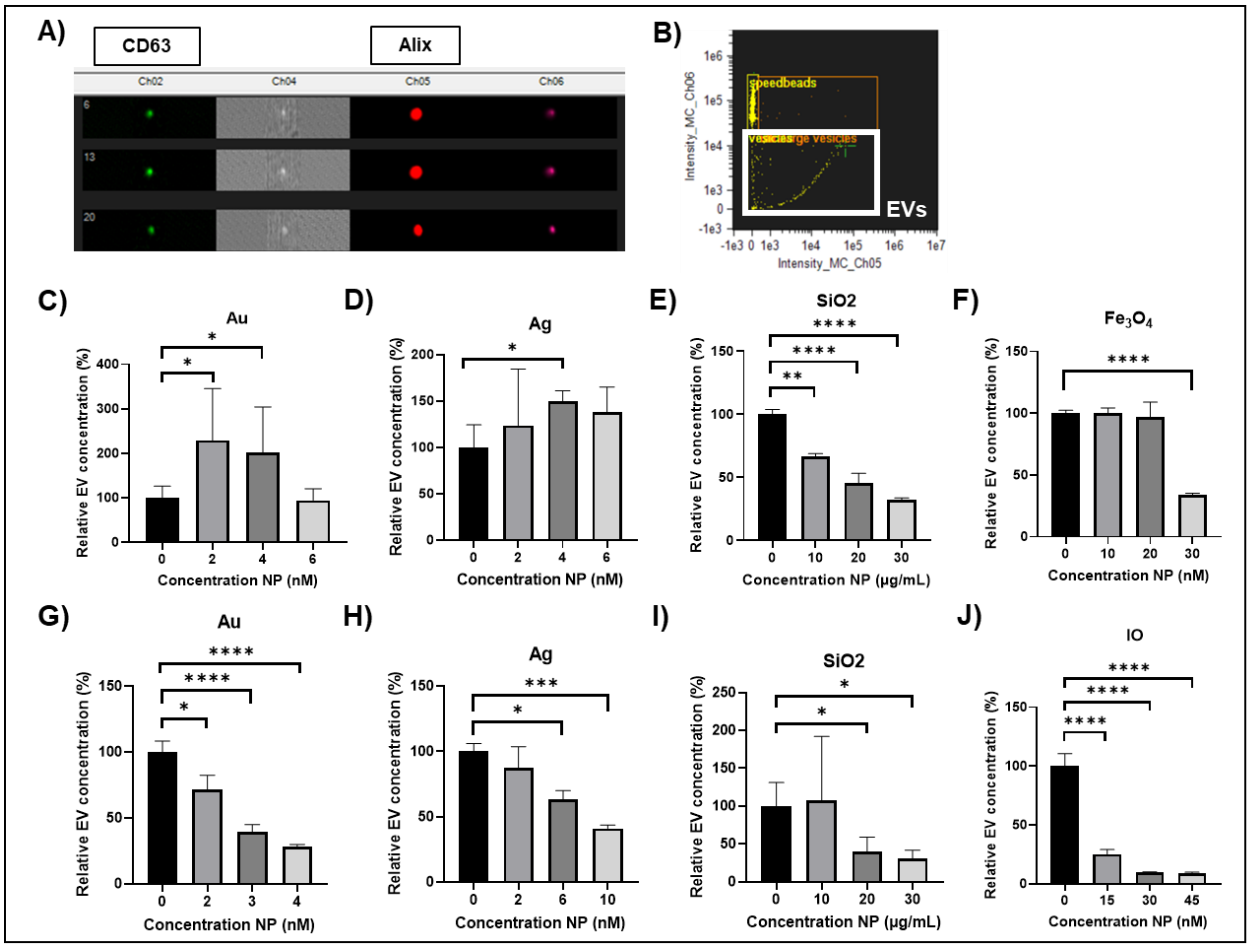


*oxide (4 nm, PMA coated) administered in MDA-MB-231 cells (C-F) and B16-F10 cells (G-J). *p<0.05 vs negative control (0 nM). Data is represented as mean ± SD (n = 5).*

**EV internalization**

We then set out to verify whether these EVs are capable of intercellular communication by analyzing whether the purified EVs are internalized successfully in potential target cells. We therefore performed an internalization study to explore the potential of purified EVs from either B16-F10 or MDA-MB-231 cell culture supernatant to be taken up by other cultured cells. Confocal analysis of fluorescently-tagged EVs exposed to B16F10 cells and MDA-MB-231 cells revealed distinct internalization of EVs by the cultured cells and furthermore indicated a clear cellular tropism, where the EVs were taken up more extensively by the cell type they originated from (**Supporting figure S2**). The latter is in line with literature, where EVs have been widely described to express surface molecules that govern their tissue homing and enable cell-specific interactions.[43] Cellular internalization was further confirmed by image-based flow cytometry, where cells incubated after 2 hrs already revealed distinct levels of EV internalization, which increased further as time progressed to 24 hrs exposure (**Figure 6, Supporting Figure S3**). As the previous confocal results demonstrated a distinct cell type-dependent preference of uptake, EVs were incubated with the same cell type they originally were obtained from. For this purpose, cultured B16F10 or MDA-MB-231 cells were exposed to medium supplemented with DiD-stained $1*10^6$ EVs/ml for the indicated time points.

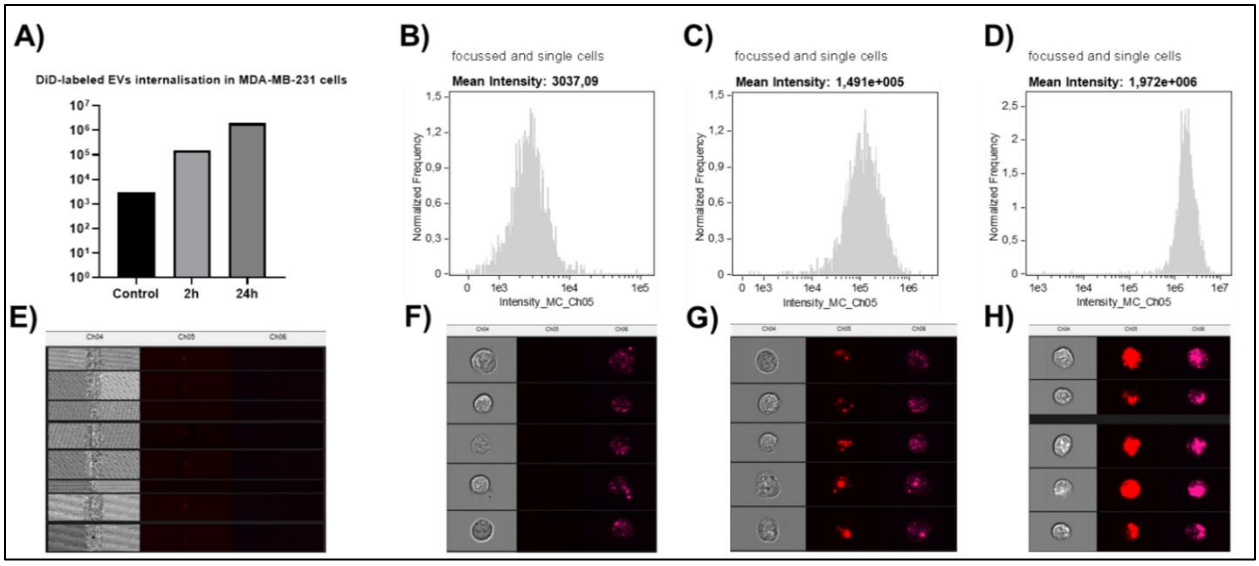


***Figure 6. Uptake of EVs.*** *Image-based flow cytometry analysis of fluorescently labeled DiD-EVs (fluorescence emitting in Ch05) taken up by MDA-MB-231 cells* ***A)*** *Summary of time-dependent uptake of DiD-labelled EVs including 3 timepoints/conditions:* ***B)*** *Control sample. Only cells, without administration of fluorescently labeled DiD-EVs.* ***C)*** *2h after DiD-EV administration* ***D)*** *24h after DiD-EV administration.* ***E)*** *shows DiD-labeled EVs derived from the respective cell types (no cells). Because of their size, EVs limited to be registered by fluorescence intensity (CH05) only. Figures* ***F-H)*** *are illustrative figures of image-based flow cytometry analysis of data shown in B-D respectively. Data is represented as mean ± SD.*

Given the cellular tropism of EVs, tumor cell-derived EVs may influence neighboring but also more distant (metastatic) tumor cells, but within the tumor

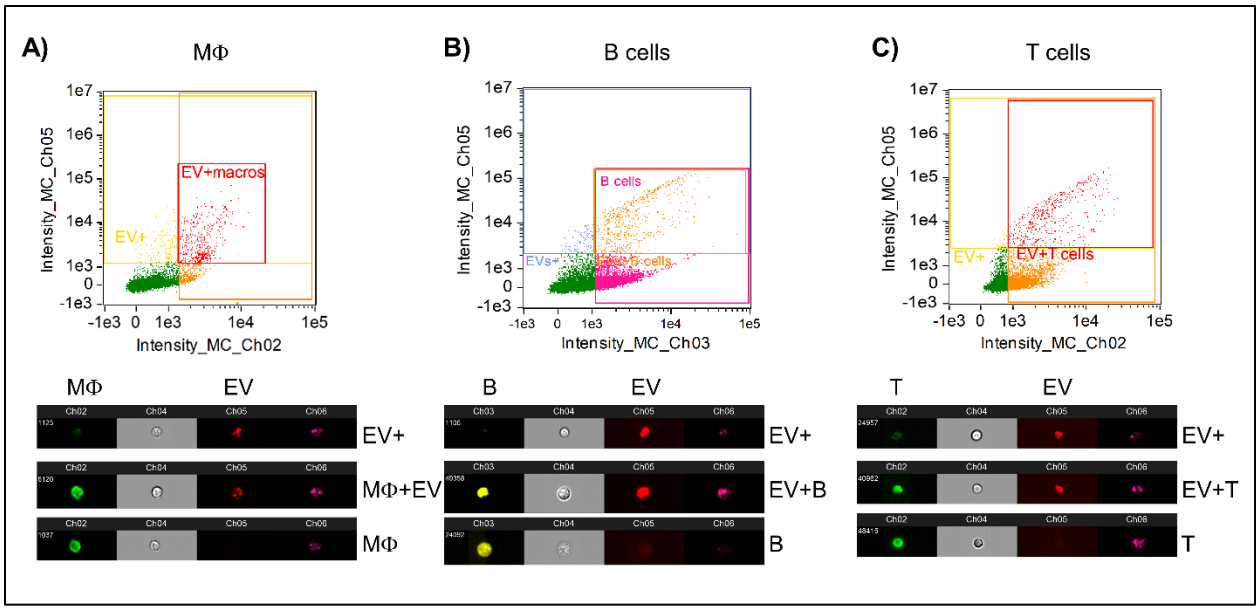

microenvironment (TME), they may also interact with other TME-resident cell types, such as tumor-associated macrophages (TAM), tumor infiltrating lymphocytes (TILs) or others (cancer-associated fibroblasts (CAFs) or tumor endothelial cells (TECs)). As EVs have been described to play a major role in immunomodulation and tumor progression,[44] and can even influence the outcome of therapeutic strategies based on immune checkpoint inhibitors,[45] the specific interaction of EVs with macrophages and lymphocytes (T-cells and B-cells) was also studied by image-based flow cytometry (**Figure 7**).

***Figure 7. EV uptake by immune cells. A-C****) Scatter plots of splenocytes incubated with fluorescently labeled DiD-EVs (fluorescence emitting in Ch05) and stained with antibodies against* ***A)*** *F4/80 (macrophages; M$\phi$),* ***B)*** *CD19 (B cells) or* ***C)*** *CD3 (T cells). The respective gating strategies are shown to indicate M$\phi$, B and T cells and to illustrate EV$^+$ from EV$^-$ cells. Below the scatter plots, are representative images of cells showing their respective fluorescence levels, brightfield (Ch04) and side scatter (Ch06) images. The images are shown for representative cells out of (top) EV$^+$ cells, not positive for antibody marker, (middle) antibody-marker positive cells containing EVs and (bottom) antibody-marker positive cells negative for EVs.*

Over time, an increased uptake of DiD-positive EVs was found in all studied cell types. Overall, around 1% of the total splenocyte population was found internalizing EVs after a co-incubation time of 2 hours. Looking into the specific cellular subtypes, 51% of macrophages ($F4/80^+$) has internalized EVs, but the macrophage population constituted only a minor fraction of the entire splenocyte isolate. For mature T ($CD3^+$) and B ($CD19^+$) cells, both had approximately 5% of their population taken up EVs. A large fraction of cells (likely a mixture of less mature B or T cells, endothelial cells and cells making up the spleen lining) had almost no EV uptake.

**miRNA analysis of cell-derived EVs**

Next, we studied whether NP exposure at subcytotoxic conditions could affect the genetic cargo that cell-derived EVs contain. To this end, the human MDA-MB-231 cells were treated for 24 hrs with Au (3 nM), Ag (4 nM), $SiO_2$ (20 µg/ml) or IONPs (20 nM), after which the cells were washed extensively to remove free NPs and incubated for 24 hrs in medium with EV-depleted FBS after which conditioned cell culture supernatant was collected and the total miRNA was collected from the EVs contained therein. EV miRNA expression patterns of 168 breast cancer-related miRNAs were then profiled. Expression analysis revealed significantly up- and downregulated miRNAs for the different NP formulations (**Figure 8**). Interestingly, the data reveal clear differences in miRNA level alterations between the various NPs, indicating that every NP formulation had a differential effect.

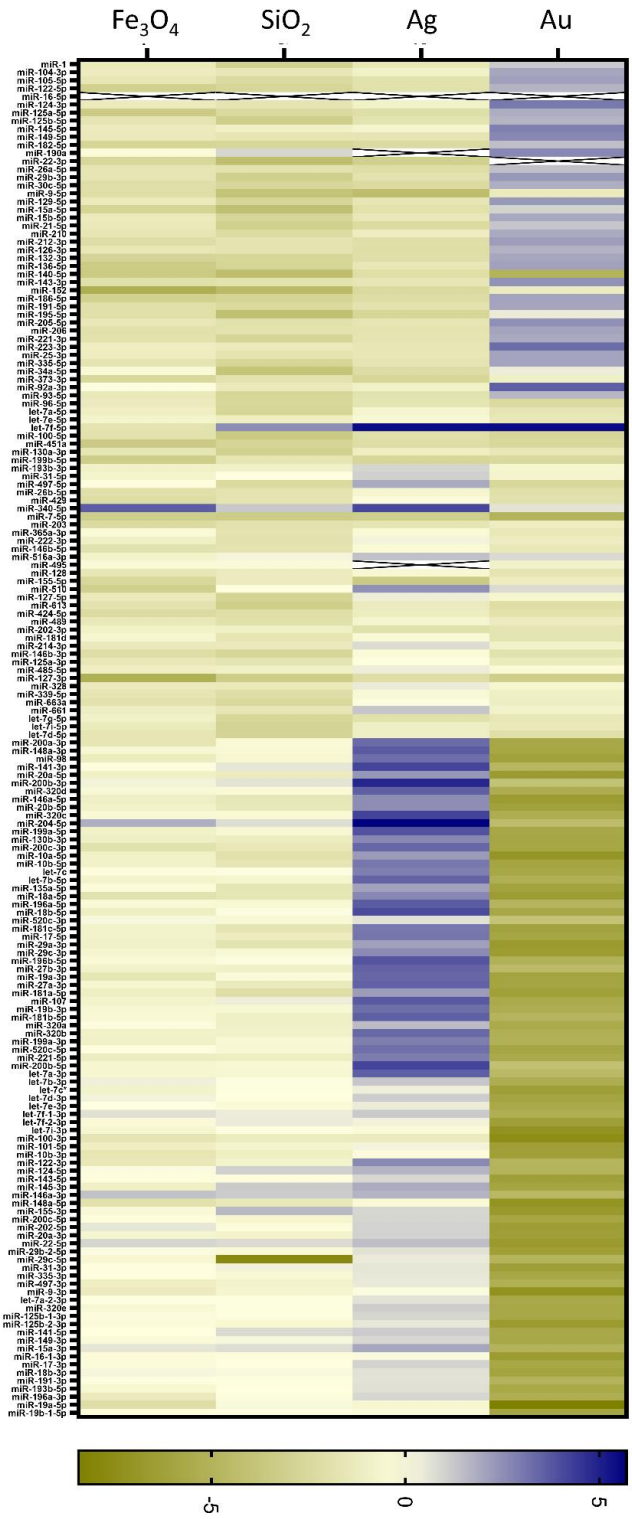


***Figure 8. Expression pattern of EV miRNA cargo.*** *Heatmap visualization of miRNA qPCR array data of miRNA expression levels found in purified EVs from MDA-MB-231 cell culture supernatant upon NP treatment. Fold-change expression levels compared to those of control (non-treated) expression levels. Relative quantification of each miRNA expression level was normalized according to the expression of housekeeping snRNA. X-axis: NP treatment, Y-axis: miRNA primer pairs.*

To evaluate the effect of miRNA expression on gene profiles, gene interaction enrichment and network analysis was performed for all miRNAs that were more than 2.75-fold different than EVs obtained from untreated control cells. Using these data, a putative list of the most likely gene interaction partners was identified for all samples (**Figure 9**) and a putative network of all known (validated) miRNA-gene interactions was assembled (**Supporting Figure S4**). When looking at the set of putative interaction genes, the 4 NPs result in widely different effects on the cells they are exposed to, as evidenced by the lack of common interacting genes between the NPs.

The extent of possible gene alterations was also highly dependent on the type of NP used, where IONPs resulted in the least dense network, followed by Ag and Au NPs while $SiO_2$ NPs had the most widespread effects on EV-mediated miRNA generation (**Supporting Figure S4**).

To gain more functional insight into these findings, functional enrichment analysis was performed, highlighting the most likely genes affected by EVs generated by cells that had been exposed to any of the NPs (**Supporting Table S1**). Interestingly, $SiO_2$ NPs, as indicated above, clearly induced miRNAs that could affect a dense network of cellular pathways (**Figures 9, 10**). Of the potential pathways involved, one group of genes that are likely affected by miRNAs upregulated through cellular exposure to $SiO_2$ NPs is associated with “nanoparticle effects”. This may be linked to our earlier hypothesis related to the $SiO_2$ NP-mediated reduction in EV generation levels, where it has been described that $SiO_2$ NPs can affect membrane fluidity levels, which in turn, may affect cellular wellbeing and in doing so, generate cell stress.

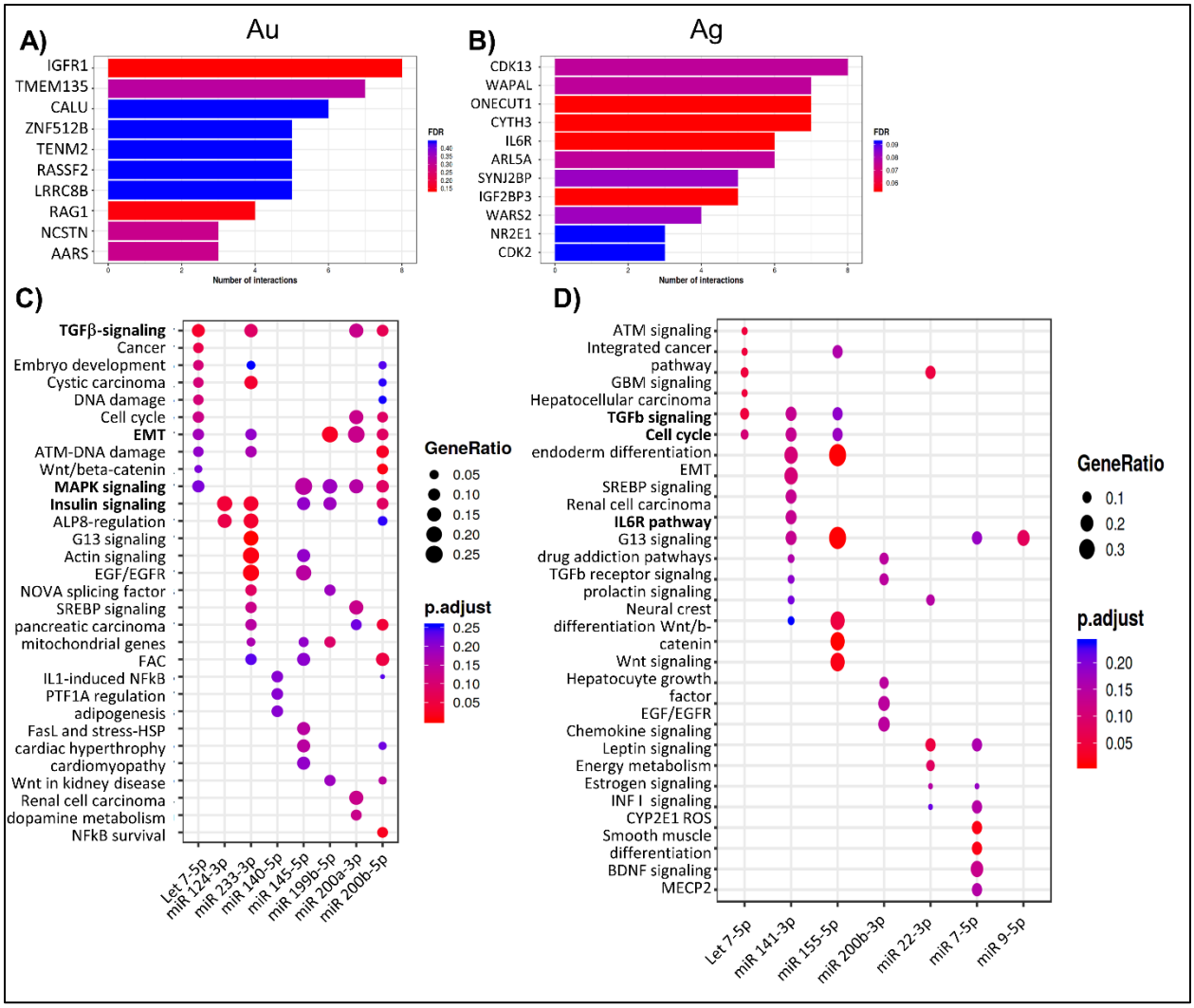


***Figure 9. Gene interaction enrichment.*** *MIENTURNET based enrichment of miRNA-target genes and pathway analysis for miRNAs obtained in EVs derived from MDA-MB-231 cells exposed to* ***A,C)*** *Au NPs,* ***B,D)*** *Ag NPs,* ***A,B)*** *Bar plots representing each miRNA resulting from the enrichment along with the number of its target genes. The color of the bars represent the adjusted p-values (FDR).* ***C,D)*** *Dot plot of functional enrichment analysis for target genes of selected miRNAs resulting from the enrichment analysis. The Y-axis reports the annotation categories through WikiPathways and the X-axis reports the selected miRNAs. The color of the dots represent the adjusted p-values (FDR), whereas the size of the dots represents gene ratio (i.e. the number of miRNA targets found enriched in each category over the number of total genes associated to that category).*

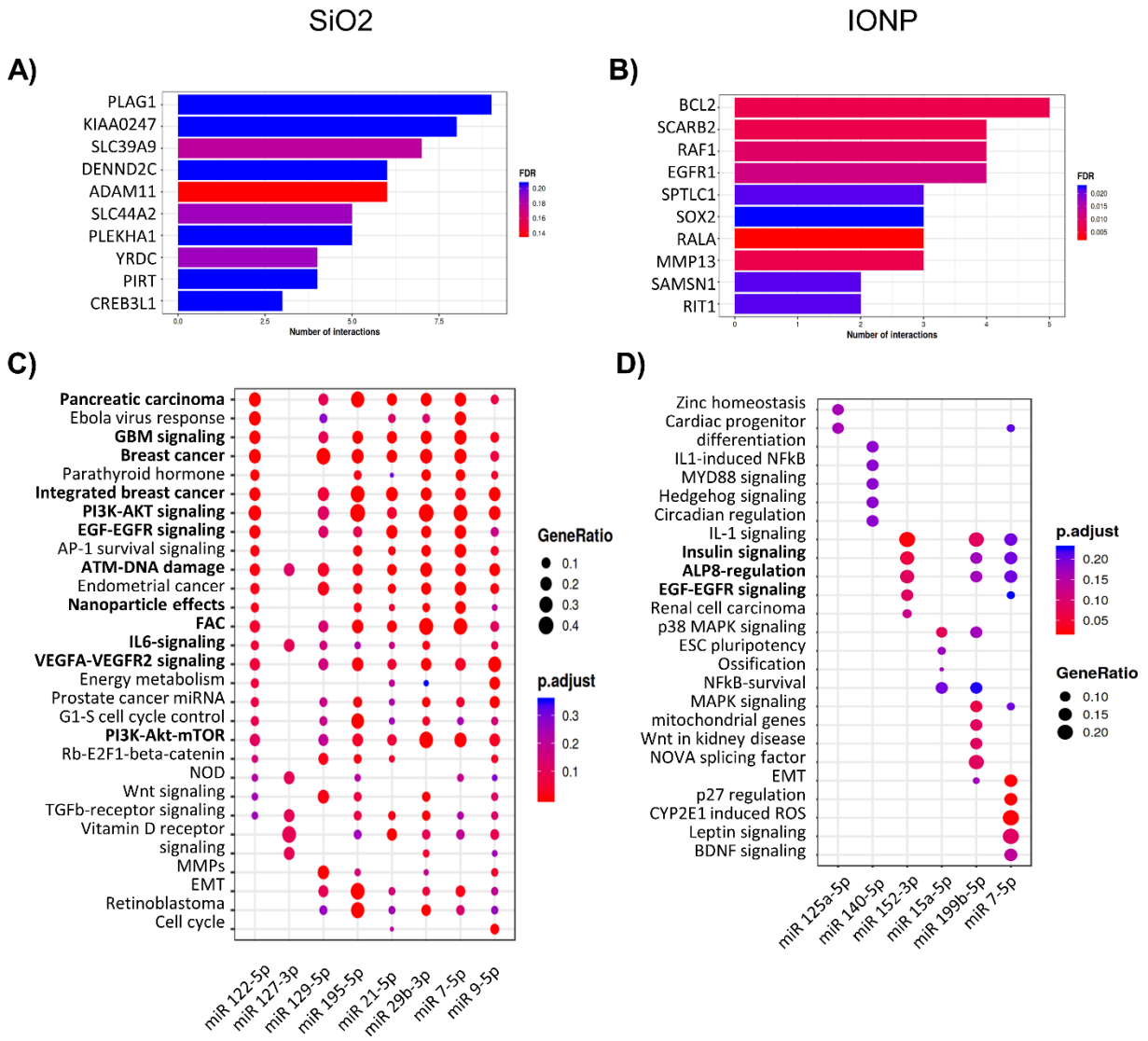


***Figure 10. Gene interaction enrichment.*** *MIENTURNET based enrichment of miRNA-target genes and pathway analysis for miRNAs obtained in EVs derived from MDA-MB-231 cells exposed to* ***A,C)*** *$SiO_2$ NPs,* ***B,D)*** *$Fe_3O_4$ NPs,* ***A,B)*** *Bar plots representing each miRNA resulting from the enrichment along with the number of its target genes. The color of the bars represent the adjusted p-values (FDR).* ***C,D)*** *Dot plot of functional enrichment analysis for target genes of selected miRNAs resulting from the enrichment analysis. The Y-axis reports the annotation categories through WikiPathways and the X-axis reports the selected miRNAs. The color of the dots represent the adjusted p-values (FDR), whereas the size of the dots represents gene ratio (i.e. the number of miRNA targets found enriched in each category over the number of total genes associated to that category).*

For $SiO_2$ NPs, many of the affected miRNAs have been found to be involved in tumor signaling, specifically breast cancer, glioblastoma and pancreatic adenocarcinoma. In view of specific pathways, the phosphoinositide 3-kinase-AKT (PI3K-AKT), epidermal growth factor (EGF)-EGF receptor (EGFR), Ataxia-telangiectasia mutated (ATM) kinase-DNA damage, interleukin (IL6) signaling and vascular endothelial growth factor (VEGF)-(VEGF) receptor A (VEGFRA) signaling pathways are strong candidates to be affected. The PI3K-AKT pathway is closely linked with cellular proliferation and cell survival. Upregulation of this pathway is typically linked with tumor progression and increased resistance against common therapies.[46] The EGF-EGFR pathway has also been linked with aggressive tumors as it can lead to increased proliferative potential, nitric oxide synthesis, and an accelerated cell cycle progression and has been commonly noted in breast carcinomas.[47] The ATM-DNA damage associated pathway plays a more complex role, where ATM is involved in oxidative sensing or DNA damage and was initially considered a major tumor suppressor as it can induce cell cycle arrest or apoptosis. However, in more advanced tumors, ATM signaling has been linked to enhanced resistance and increased progression and malignancy.[48] IL6 signaling protects tumor cells from oxidative stress and apoptosis, and has been associated with an increased level of malignancy.[49] The VEGF-VEGFRA pathway: VEGF correlates with invasiveness, vascular density and metastasis levels, where increased VEGF release by tumor cells can stimulate endothelial cell progression and result in the formation of new blood vessels, which may be structurally abnormal and leaky.[50] Overall, for $SiO_2$ NPs, our findings would suggest that the NPs may affect tumor physiology, and in particular, could promote tumor progression or metastasis. While limited data is available on the tumor effects of $SiO_2$ NPs, a recent study suggested that inflammation induced by $SiO_2$ may indeed be tumorigenic.[51] $SiO_2$ have also been linked to increased metastasis levels, but this was in a cancer cell-unrelated process. Specifically, $SiO_2$ have been linked with increased tumor vessel permeability by

creating pores through which tumor cells can extravasate. However, a more recent study indicated that upon functionalizing the surface of $SiO_2$ NPs with poly(ethylene glycol) (PEG), these effects were lost.[52] Overall, it remains unclear to what extent $SiO_2$ NPs may affect tumor progression or malignancy, but the data provided here suggests that this should be looked into further.

For IONPs, the extent of miRNA alterations was far lower resulting in particular in EGF-EGFR, alkaline phosphatase (ALP8) and insulin signaling pathways being affected. For EGF-EGFR, this will be similar as for the $SiO_2$ NPs, where it is linked with aggressive tumors and an increase in tumor progression. The ALP pathway is less well described as the function of alkaline phosphatase, best known as a serum marker for liver damage, remains somewhat poorly understood. Some studies have highlighted the involvement of ALP processes as cell growth, apoptosis and cell migration during embryonic development.[53] A recent study confirmed these effects on tumor cells, where elevated ALP levels correlated with increased cell migration and reduced cell death.[54] The insulin pathway is well-known to be involved in cell metabolism and glucose processing. The link with cancer itself remains somewhat unclear, but several studies have suggested that high insulin levels can result in tumor development. Mechanistically, hyperinsulinemia can result in insulin binding to insulin-like growth factor receptor (IGFR),[55] which has been shown to result in increased resistance of breast adenocarcinomas to chemotherapy .[56] Together, these data reveal a potential role of IONPs in tumor physiology, although this has not been directly reported in literature. The latter may be due to the fact that for IONPs, most studies have focused on their efficient sequestration by tumor-associated macrophages (TAMs) and their subsequent polarization of TAMs from an anti-inflammatory to a pro-inflammatory state. This makes IONPs efficient tools to combat cancer through immune therapy and also highlights the importance of deciphering the exact role and complex

behavior that NPs, like many common chemotherapeutic agents, may have on tumor physiology.

**Effects of Ag NP-affected EV-miRNA on tumor physiology**

For Ag NPs, the IL6 pathway was affected, similarly as for $SiO_2$ NPs. However, unlike for $SiO_2$, where the miRNAs affected will increase IL6-mediated signaling, the miRNAs affected by Ag NPs will decrease IL6-mediated signaling. This finding is quite interesting, as IL6 has been suggested as a therapeutic target in cancer immunotherapy as tumor-induced IL6 has been found to inhibit immune cell activation during cytotoxic chemotherapy.[57] Ag NPs themselves have also been described to synergistically enhance therapeutic efficacy when used in combination with various chemotherapeutic agents, including cisplatin and camptothecin.[58] We then sought to evaluate whether Ag NPs would be able to induce immune cell responses to cancer cells and whether EVs would play a role in this. To test this, B16F10 cells were exposed to Ag NP at subcytotoxic conditions, after which the media were removed and cells were kept for another 24 hrs in order to generate EVs that could be collected. Media of the different conditions were then used and processed as described in the Experimental section after which the B16F10 media were used to stimulate primary monocytes. In total, 4 conditions were tested, comprising either monocytes exposed to B16F10-conditioned medium 1) in the absence of Ag NPs, 2) in the presence of Ag NPs, 3) in the presence of Ag NP-affected EVs, 4) in the absence of Ag NP-affected EVs (**Figure 11, Supporting Figure S5, S6**).

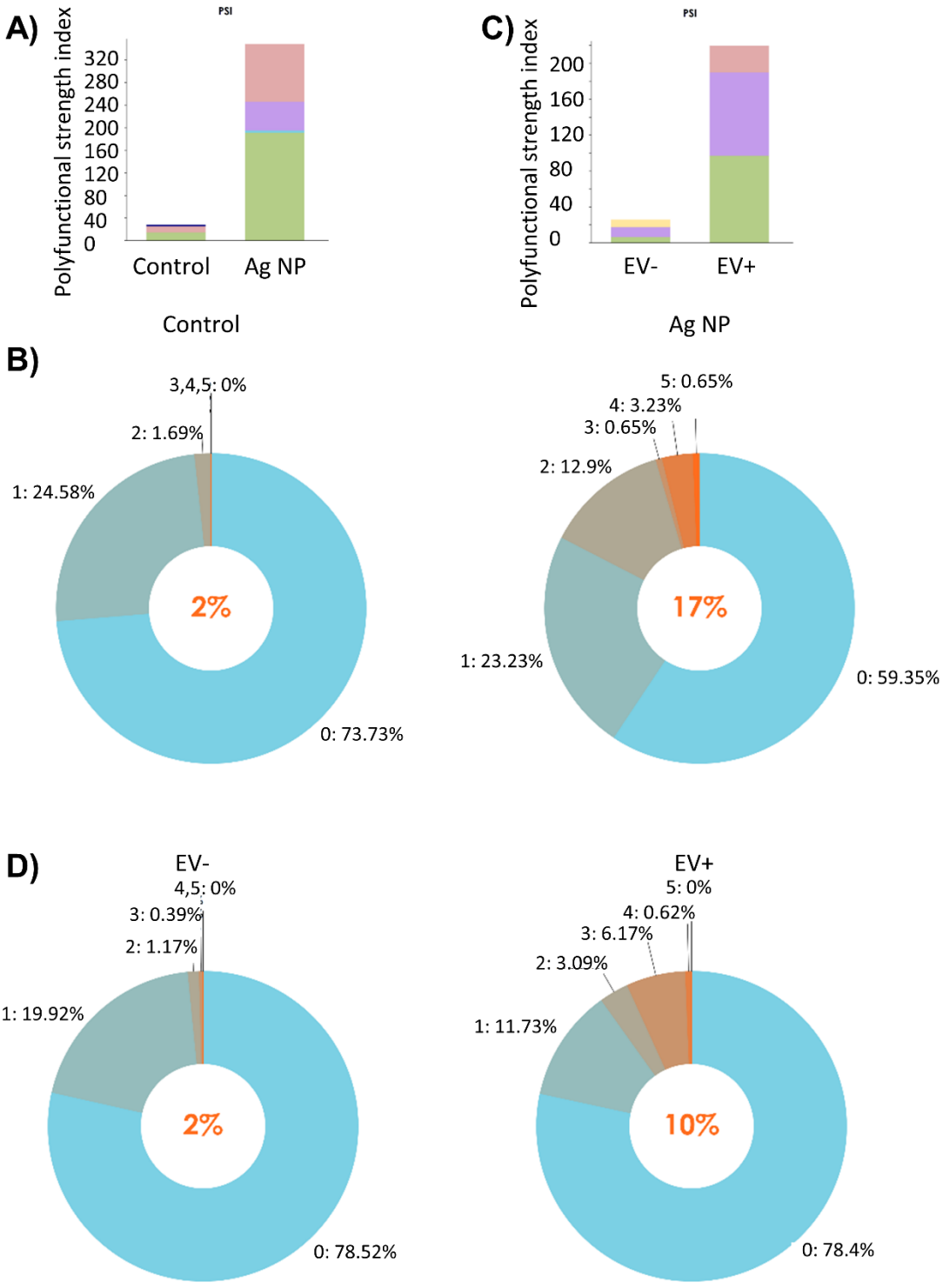


***Figure 11. Ag NP induced immune response.*** *Murine monocytes were incubated with conditioned medium from B16F10 melanoma cells either* ***(A,B)*** *left untreated (control) or in the presence of Ag NPs,*

*or **(C,D)** in medium obtained from B16F10 cells previously exposed to the Ag NPs upon removal in the NPs but in the absence (EV-) or presence (EV+) of B16F10-secreted EVs. **A, C)** The polyfunctional strength index indicated by relative abundance and composition of secreted cytokines and **B, D)** the relative polyfunctional distribution split as the percentage of cells with 1, 2, 3, 4, 5 or more cytokines expressed. Data is represented as mean for 3 independent repeats.*

The data reveal a low level of polyfunctionality (2%) in both control conditions and EV- conditions. However, when monocytes were exposed to conditioned medium containing Ag NPs, a clear increase in polyfunctionality (17%) was observed, suggesting that Ag NPs at subcytotoxic conditions on their own, indeed, can activate monocytes, either directly, or indirectly, through cancer cell-mediated signaling molecules. The lack of any polyfunctionality increase in EV-depleted medium suggests that the observed effects are possibly through Ag NPs themselves, but are not caused by growth factors or other small molecules induced by the Ag NPs in the B16F10 cells. In the EV-containing medium, polyfunctionality was increased up to 10%, which is far higher than for control or EV-depleted medium, but not as high as for Ag NP-containing medium. The data furthermore indicate that for both Ag NPs and EVs, the cytokines induced are mainly effector ones (TNFα), chemoattractive (MIP-1b, IP10) or inflammatory (MIF, MCP-1). As illustrated in Figure 11B,D, the EVs mainly resulted in an increase in chemoattractive chemokines, which would stimulate the influx of other immune cells, while the Ag NPs themselves resulted more strongly in inflammatory signals. Together, these data reveal that Ag NPs have a strong immunostimulatory effect which is very likely to support cancer immunotherapy. Additionally, EVs generated by the Ag NPs themselves are also able to induce a pro-inflammatory TME, which is beneficial for immunotherapy. Therefore, EVs seem to play an important role in enhancing the signal elicited by the Ag NPs as only a single cancer cell can generate many EVs which can transmit the associated miRNA-loaded EVs to surrounding tumor or immune cells in the TME.

**Effects of Au NP-affected EVs on tumor physiology**

For Au NPs, the most affected pathways were related to insulin signaling, mitogen-activated protein kinase (MAPK) signaling, epithelial-to-mesenchymal transition (EMT) signaling and transforming growth factor β (TGFβ) signaling (Figure 9A,C). Insulin signaling, as indicated for the IONPs, is somewhat unclear, but may be associated with enhanced chemoresistance. MAPK signaling is an important pathway in cell survival and cell growth and increased expression results in uncontrolled cell proliferation and resistance to apoptosis, which can result in increased chemoresistance.[59] EMT is the process that tumor cells undergo to go from an epithelial to a mesenchymal state, which increases its mobility. It is therefore heavily associated with metastasis and is seen as a natural process that tumor cells can undergo prior to metastasis formation.[60] TGFβ signaling is slightly more complex, where TGFβ has been linked with tumor suppression through its role in regulating cell proliferation and controlling apoptosis.[61] However, TGFβ has also been linked with an immunosuppressive TME which impedes immunotherapy, and furthermore increase therapeutic resistance, stem cell properties of tumor cells and metastatic dissemination.[62] The latter is partly in line with the EMT pathway involvement as TGFβ is a known potent inducer of EMT.[63] Interestingly, both TGFβ and EMT signaling were found to be downregulated by the Au NP-affected miRNAs. Together, these data suggest that Au NPs may impede cell migration. Literature data has indeed shown that Au NPs themselves can indeed affect cell mobility.[64] To evaluate the potential effect of Au NPs on cell migration and the role of EVs in this effect, MDA-MB-231 cells, previously exposed to conditioned medium from cells that were left untreated, exposed to Au NPs, or to media with or without EVs generated by Au NP-treated cells were seeded in transwell plates after which cellular migration was counted in view of FBS as a chemoattractant. The data reveal that Au NP-treated cells were significantly less mobile than control cells (**Figure 12**). Interestingly, in conditioned medium without

EVs, little to no effect on cellular migration was observed, whereas EV-containing conditioned medium also had a significant decrease in cellular mobility, although the

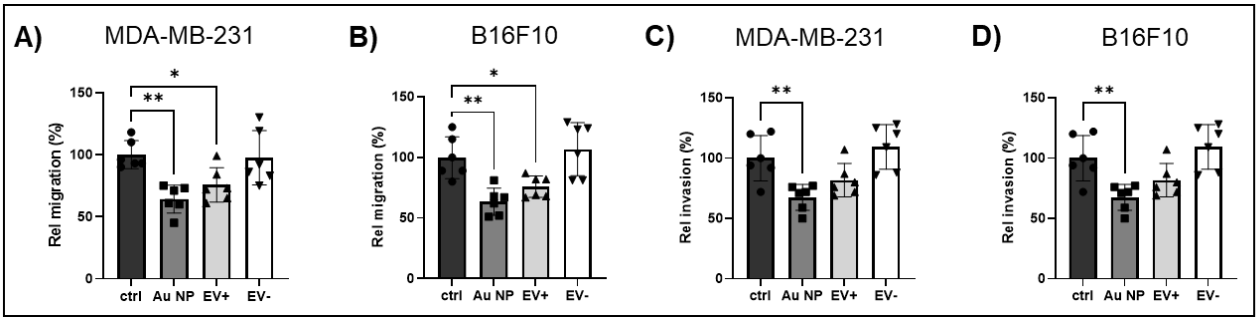


effect was not as strong as observed for Au NP themselves.

***Figure 12. Au NPs affect migration and invasion levels.*** *Histograms representing* ***A,B)*** *relative cell migration and* ***C,D)*** *relative cell invasion levels for MDA-MB-231* ***(A, C)*** *and B16F10* ***(B,D)*** *cells either left unexposed (ctrl), or exposed for 24 hrs to Au NPs (Au) or conditioned medium of cells previously exposed to Au NPs, without any NPs remaining, but in the presence (EV+) or absence (EV-) of cell-secreted EVs. The data are expressed as mean ± SD (n = 6) relative to the level for untreated control cells (100%). The degree of statistical significance is indicated when relevant (*p < 0.05; **p < 0.01).*

## STUDY CONSIDERATIONS

The present study clearly revealed the impact that different NPs may have on tumor cells, as well as on the genetic cargo of tumor cell generated EVs. Interestingly, given the precise physicochemical properties of the NPs, this can have either potentially negative effects, but can also result in miRNA alterations that can be of therapeutic interest. One limitation of the current study is that while the NPs were characterized as much as possible with the available instrumentation for us, additional characterization such as elemental analysis of crystal structure, see, for example Zhang et al.[65] could also provide more insights into the precise nature of the NPs and their biological effects. While it is outside of the scope of the current study, it would be interesting to look at the effect of 'contaminants' or alterations in crystal structure in view of their effects on EV synthesis and molecular changes. While the impact of EVs is never as strong as that of NPs on their own, the data obtained here suggests that EVs can greatly amplify any NP-elicited physiological change. The present study aims to provide a small step towards our understanding of how secondary signaling molecules such as EVs can explain any changes observed upon NP administration to cell *in vitro*, or in particular in preclinical animal models. While this study sheds some light on the need to carefully consider EVs and their role in NP toxicity, it can thus also be exploited to tailor NP therapeutic efficacy. However, great care needs to be taken upon interpreting the results reported here as it is not possible to draw any general conclusions. Firstly, the studies performed here are happening on cultured cancer cell lines, and may therefore differ from the multicellular environment of the TME. We mainly looked at the impact of EVs on other cancer cells, but as shown for the Ag NPs, they can also directly affect immune cell populations, which is well-known in literature[66,67]. Apart from the multicellular composition of the TME, another important component to consider is the relatively low number of cells in the TME that actually interact with administered NPs[68]. Therefore, the relative number of altered versus

unaltered EVs *in vivo* compared to *in vitro* conditions will likely be quite different. Secondly, the NPs used here are of different chemical composition, but also have different size and different surface coating. As it is known that all these parameters play a major role in the toxicological profile of NPs, the results obtained here for a particular formulation may not be observed for other NP formulations. This is also true for the cell models used, where in this case, the observations in the two cancer cell lines, will not be identical for all cell types. In particular with regard to the miRNA alterations, this will be heavily dependent on the cell type used as different signaling pathways and cellular responses which are heavily linked to particular cellular lineages will play a role in which miRNAs will be more prevalent. One other limitation in the present study is that the effects here, as in most NP or EV-based studies have specifically looked at short-term effects and therefore do not address the possible risks associated with the long-term exposure to either of these entities. While EVs are generally biodegradable, various inorganic NPs are not readily degrading and can therefore cause more pronounced long-term effects, also on the level of EV secretion and EV functionality.

## Conclusion

To summarize, in this study we have investigated and confirmed that inorganic NPs can significantly increase or decrease EV secretion levels in MDA-MB-231 cells and induce alterations in their specific genetic miRNA EV cargo. Specifically, miRNAs can function as posttranscriptional regulators of genes involved in metastasis formation.[69] As such, upon the confirmed successful uptake of these EVs, this could lead to the induction of phenotypic alterations in target cells. In this study, we demonstrated clear cell type and nanomaterial type related differences in view of EVs synthesis levels and the molecular cargo loaded inside EVs obtained from cells previously exposed to the NPs. It is important to note that the levels of generated EVs can be increased or impeded by the same NP, depending on the concentration used or cell type which is exposed to them. The NP-elicited alterations in EV miRNA cargo can have profound effects, as shown by the anti-cancer immune activation through Ag NP-induced EVs. However, also here, the effects can differ per cell, where MDA-MB-231 cells displayed significantly reduced invasive properties upon Au NP exposure or exposure to Au NP-elicited EVs, while in B16F10 cells, significant effects were only observed for the NPs themselves, and not for NP-elicited EVs. Together, these data highlight the need to further unravel the precise interactions of engineered NPs and EVs, and to also focus on the role of EV-mediated signaling in view of potential toxicity or therapeutic success of nanomedicines.

## Experimental section

### *Nanoparticles and nanoparticle characterization*

In the present study, we made use of four biomedically relevant nanoparticles: gold (20 nm, polymer coated), silver (4 nm, PMA coated), silicon dioxide (30 nm, -COOH coated) and iron oxide (4 nm, PMA coated). The gold and silicon dioxide nanoparticles had been purchased commercially (NanoComposix, Ltd), while the silver and iron oxide particles were obtained through collaborations with the group of Wolfgang Parak (University of Hamburg). We intentionally incorporated nanoparticles of different natures and sizes in this study to compare their effects. Further, our nanoparticle type selection was guided by literature findings and preliminary results from our research group.

All nanoparticles in this study were characterized using Transmission electron microscope (TEM) to determine their shape and size, Dynamic light scattering (DLS) to measure hydrodynamic diameter and surface charge, zeta potential analysis, and Nanoparticle tracking analysis (NTA) for evaluation of colloidal stability.

*TEM*

Formvar film coated 400-mesh copper grids (Agar Scientific Ltd., England) were used. To improve adsorption efficacy of the nanoparticles, the grids were originally glow-discharged. Nanoparticle dilution samples of 25 µL were loaded on the grids and left to evaporate. Finally, images were acquired using a JEM-1400 transmission electron microscope (JEOL, Japan) at an accelerating voltage of 80 keV.

*DLS*

Dynamic light scattering (Malvern Panalytical, Zetasizer Nano ZSP, United Kingdom) was applied to define hydrodynamic size distribution, polydispersity index (PDI) and Zeta potential of the nanoparticles. Samples were diluted in PBS. Measurements were

performed at 25°C, registering light scattering intensity at an angle of 90°. For each sample, an average of 3 measurement series was established.

*NTA*

Nanoparticle tracking analysis was performed using a NanoSight NS300 system (Malvern, UK) to determine average NP size and concentration (particles/mL). Diluted samples were introduced by a pump-controlled syringe and in total, five videos of 30 s each sample were captured at a frame rate of 25 frames/second. Particles were tracked using NTA 3.0 software (Malvern Instruments GmbH) at camera level 10 and appropriate detection threshold (4).

***Cell lines***

For this study, MDA-MB-231 triple-negative human breast cancer cells were cultured in high glucose containing Dulbecco's modified Eagle's medium (DMEM), supplemented with 10% Fetal Bovine Serum (FBS) and 1% penicillin/streptomycin (Gibco, Invitrogen, Belgium) under a humidified atmosphere at 37 °C and 5% $CO_2$ and split upon a 1:4 subcultivation ratio 2 to 3 times a week at 80% confluency. B16-F10 murine melanoma cells were cultured in Roswell Park Memorial Institute (RPMI) medium, supplemented with 10% Fetal Bovine Serum (FBS) and 1% penicillin/streptomycin (Gibco, Invitrogen, Belgium) under a humidified atmosphere at 37 °C and 5% $CO_2$ and split upon a 1:10 subcultivation ratio 2 to 3 times a week at 80% confluency.

***Cell-Nanoparticle interaction studies - in vitro high-content analysis***

MDA-MB-231 or B16F10 cells were seeded at 4000 cells/well in 96 well plates (Corning Costar, Thermofisher scientific, USA) and allowed to attach overnight under a humidified atmosphere at 37 °C and 5% $CO_2$. Cells were then incubated with a range of increasing NP concentrations for 24h in complete growth medium. Conditions were applied in triplicates. High content imaging analysis was performed based on

previously described and validated methods, in which cell viability and mitochondrial reactive oxygen species were measured as described.[31]

***Purification of Extracellular vesicles upon NP exposure***

*Preparation of concentrated conditioned medium (CCM)*

Extracellular vesicles were isolated from concentrated conditioned medium (CCM) derived from cell culture supernatant of MDA-MB-231 cells or B16-F10 cells grown at 70% in T182.5 flasks. After several washing rounds of seeded cells with serum-free medium, cells are treated with a subtoxic range of each of the 4 inorganic nanomaterials (gold, silver, silicon dioxide, iron oxide) for 24 hrs, after which the medium is removed, cells are extensively washed to remove any remnant NPs and the cells are then left to incubate with medium containing EV-depleted FBS for an additional 24 hrs. To prepare CCM, cells were washed three times in total. A first washing step with DMEM (Gibco, Invitrogen, Belgium) (without supplemented serum) was followed by two washing steps of respectively 10 and 60 minutes with DMEM supplemented with 0.5% of EV-depleted serum (EDS). EDS was prepared by ultracentrifugation of fetal bovine serum (FBS) (Gibco, Invitrogen, Belgium) for 18 hrs at 100,000 x g at 4°C (SW55 Ti rotor, Beckman Coulter, USA), and filtered after at 0.22 µm. Subsequent to the washing steps, cells were incubated in DMEM supplemented with 0.5% of EDS for 24 hrs under a humidified atmosphere at 37 °C and 5% $CO_2$. Cell culture supernatant was then harvested and centrifuged for 10 min at 300 x g and 4°C to remove cells and debris. The supernatant was filtered after at 0.45 µm and concentrated using 10 kDa centrifugal filter units (10 kDa Amicon Ultra (Merck Millipore, USA)) at 4000 x g (swinging bucket 5810 R - Benchtop Centrifuge, Eppendorf, Germany).

*Extracellular vesicles isolation by commercially available isolation kits*

Isolation of extracellular vesicles was performed using the ExoEasy kit (Qiagen, Germany). This kit is based on a membrane-based affinity spin column binding step to isolate exosomes and other EVs from, in our case, cell culture supernatant. The membrane bound exosomes were then washed with the provided washing buffer, and finally, eluted in 400 µl of provided elution buffer (an aqueous buffer containing primarily inorganic salts).

***Characterization of Extracellular vesicles***

To standardize for the applied EV isolation protocol, quality and quantity of purified vesicles was determined by a range of different methods according to the Minimal Information for Studies of Extracellular Vesicles (MISEV) guidelines. Physical characterization was performed by Nanoparticle tracking analysis and electron microscopy, while protein content was verified using western blot.

*NTA (concentration & size determination)*

EV concentration (number of particles/mL) and median vesicle size were determined by nanoparticle tracking analysis (NTA) (Malvern NanoSight NS300, Malvern Panalytical, United Kingdom). Samples were introduced by a pump-controlled syringe and in total, five videos of 30s each sample were captured at a frame rate of 25 frames/second. Particles were tracked using NTA 3.0 software (Malvern Instruments GmbH) at camera level 10 and appropriate detection threshold.

*Western blot (protein identification)*

Samples were lysed in radio immunoprecipitation Assay (RIPA) lysis buffer (Sigma-Aldrich, USA) by six intermittent vortex repetitions over a total time range of 30 minutes. Protein concentration was determined using BCA (Pierce) assay (Thermofisher Scientific, USA). Initial sample input was set at 50 µg of total protein.

Consecutively, samples were reduced and boiled at 95°C in reducing sample buffer. Proteins were separated by SDS-polyacrylamide gel electrophoresis (SDS-PAGE) and transferred to nitrocellulose membranes (Merck Millipore, USA). Membranes were blocked using 5% non-fat dried milk in PBS (blocking buffer) and washed three times in PBS (pH 7.2) including 0.1% Tween 20 (washing buffer). Membranes were then incubated with primary antibody (1:1000) in blocking buffer overnight at 4°C under permanent agitation. The next day, membranes were washed three times with washing buffer and incubated with secondary antibody (1:5000) in blocking buffer

for 1 h at room temperature under permanent agitation. Finally, membranes were washed three times with washing buffer and blotted bands were developed and visualized by chemiluminescence (SuperSignal™ West Pico PLUS, Thermo Scientific, USA).

*Electron microscopy (shape and size determination)*

EVs were adsorbed onto the carbon side of Formvar film coated 300-mesh carbon/copper grids (Agar Scientific Ltd., England) and left to evaporate for 5 min at RT. Grids were negative stained with 25 µL 2 % uranyl acetate (diluted in filtered MiliQ water) for 1 min. After drying the samples, images were acquired on a JEM-1400 transmission electron microscope (JEOL, Japan) at an accelerating voltage of 80 keV.

***Quantitative EV analysis using image-based flow cytometry***

Purified extracellular vesicles were double-labeled using 1:200 CD63-FITC fluorophore conjugated antibody and 1:200 Alix-AF647 conjugated antibody (Santa Cruz Biotechnology, USA) and registered using an image-based cytometer (Imagestream Mark II Imaging flow cytometer, Luminex, USA). During acquisition, focused and single objects were selected and gated. This was followed by gating for extracellular vesicles: Separation from speadbeads with similar sizes was performed based on the positive fluorescent labelling of EVs and separation from larger vesicles was established based on size. Collected ImageStream data was analyzed by iDEAS software (Amnis Corporation, USA), for which appropriate gating strategies were applied in order to detect double-labeled particles only. Finally, extracellular vesicles were defined as double positive for CD63 and Alix.

***RNA isolation***

Extraction of total RNA (including miRNA) from extracellular vesicles purified from CCM originating from 8 large (T182.5) cell culture flasks was performed using the exoRNeasy kit (Qiagen, Germany) based on Qiazol lysis reagent (Qiagen, Germany).

RNA was finally eluted in 14 µL of RNase free water. Total RNA concentration was determined by spectrophotometry using the Nanodrop (ND-1000 Spectrophotometer, IsoGen Life Science, the Netherlands).

***miRNA analysis of cell-derived EVs***

EV miRNA expression patterns of breast cancer-related miRNAs were profiled using the miProfile™ human breast cancer miRNA qPCR array (Genecopoeia, USA) including 168 unique miRNA primers pairs, positive and negative controls. Quantitative real-time PCR was performed using a StepOnePlus™ qPCR instrument (Applied Biosystems, USA) and All-in-one miRNA qPCR mix kit (Genecopoeia, USA) with 1 µl of cDNA input per well. 1 µg of total RNA was used for cDNA synthesis using the All-in-one miRNA First-Strand cDNA Synthesis kit (Genecopoeia, USA). cDNA is added in a 1:10 dilution to the qPCR mix. Cycle threshold (Ct) values were compared between control samples and samples that were exposed to nanoparticles for all miRNA sequences represented in the array. For further analysis of the miRNA expression profiles, the freely available MicroRNA ENrichment TURned NETwork (MIENTURNET) was used.[70] Via MIENTURNET, miRNA target enrichment analysis was performed on those miRNAs that had shown more than 2.75-fold difference in expression level than EVs obtained from untreated control cells using predicted (TargetScan) and validated (MiRTarBase) databases. Network analysis was then performed to display the miRNA's and affected genes and their regulatory pathways in order to prioritize involved interactions. Functional enrichment analysis was then performed on the top half of the miRNAs using the WikiPathways annotation database.[70]

***EV uptake***

Cellular internalization of purified EVs was verified by labelling them with Vybrant DiD dye (Thermofisher Scientific, USA) at 50 µM for 15 minutes at 37°C. DiD-Labeled EVs were then washed with PBS and purified using 10 kDa centrifugal filter units (10 kDa

Amicon Ultra (Merck Millipore, USA)) at 4000 x g (swinging bucket 5810 R - Benchtop Centrifuge, Eppendorf, Germany) to remove excess of DiD dye and concentrate the EVs. The EVs were then counted using NTA after which the EVs were administered *in vitro* to seeded MDA-MB-231 cells or B16-F10 cells. Cellular uptake of EVs is registered via image-based flow cytometry (Imagestream Mark II Imaging flow cytometer, Luminex, USA). Gating strategies were applied in order to select for focused and single objects. Data was further analyzed by iDEAS software (Amnis Corporation, USA).

***Confocal microscopy***

Cells were cultured and attached on sterile glass coverslips in 6 well plates. At 70% confluency, ExoGlow (ExoGlowTM Green, System Biosciences, USA) labeled EVs were co-incubated with the cells for the indicated amount of time. Cells were washed with Hank's Balanced Salt Solution (HBSS) (Gibco, Invitrogen, Belgium) and fixed at room temperature with 2% para-formaldehyde (PFA) for 10 minutes. Subsequently, cells were permeabilized using 1% Triton-X (Sigma-Aldrich, USA) for 10 minutes. Cells were stained at room temperature using 1:25 Actine-Phalloidin 555 in HBS for 90 minutes in dark conditions. Finally, Hoescht 33342 (Thermofisher, USA) was applied for 5 minutes at room temperature and coverslips were mounted on a glass slide. Images were acquired using Zeiss LSM 880 with Airyscan confocal microscope and analyzed using Fiji (ImageJ) software.

***IsoPlexis multiplexed cytokine analysis***

B16F10 cells were seeded at a density of 100,000 cells in 25 $cm^2$ culture flasks in full medium and exposed to pure medium or medium supplemented with Ag NPs (5 nM) for 24 hrs. The media were then removed, and kept for later use (see below). Cells were then washed and kept in low-serum containing conditions for 24 hrs. The medium was then aspirated and split in 2 parts. Half of it was kept for further use

directly, the other half was ultracentrifuged to remove any EVs (100,000 g for 18 hrs at 4°C) prior to further use. In a final step, freshly isolated monocytes (from C57Bl6 mice using the monocyte isolation kit (StemCell Technologies, Canada)) were again seeded at a density of 100,000 cells in 25 $cm^2$ culture flasks in IMDM medium supplemented with 10%FBS, 1%Pen-Strep and 0.05 mM 2-Mercaptoethanol and incubated for 24 hrs with a 50/50 volume of conditioned medium (condition 1: cells not exposed to Ag NPs), conditioned medium containing 5 nM Ag NPs (condition 2: cells exposed to Ag NPs), conditioned medium containing EVs (condition 3: medium containing EVs of cells previously exposed to Ag NPs) or in conditioned medium not containing EVs (condition 4: ultracentrifuged medium containing EVs of cells previously exposed to Ag NPs) in the presence of 10 µg/ml of LPS. In preparation for their loading into the IsoCode chips supplied by IsoPlexis (USA), the cells were washed with 1X PBS and stained with Cell Stain 405 (Isoplexis, USA) as per company protocol, after which the cells were counted, centrifuged and resuspended in complete medium without 2-Mercaptoethanol to a density of 7.5 x $10^5$ cells/ml. 40 µl of the cell suspension was loaded onto the IsoCode chips and into the Isoplexis instrument and analysis was performed on murine multiplexed cytokine analysis chips as per the company protocol.

***Cellular migration and invasion studies***

MDA-MB-231 and B16F10 cells were seeded at a density of 100,000 cells in 25 $cm^2$ culture flasks in full medium and exposed to pure medium or medium supplemented with Au NPs (5 nM) for 24 hrs. The media were then removed, and kept for later use (see below). Cells were then washed and kept in low-serum containing conditions for 24 hrs. The medium was then aspirated and split in 2 parts. Half of it was kept for further use directly, the other half was ultracentrifuged to remove any EVs (100,000 g for 18 hrs at 4°C) prior to further use. Both B16F10 and MDA-MB-231 cell lines were then seeded in 25 $cm^2$ collagen-coated tissue culture flasks at 1 * $10^5$ cells/flask and

allowed to attach overnight. Next, cells were incubated for 24 hrs with pre-conditioned medium (10 ml) obtained from the different conditions as described above: condition 1: conditioned medium of cells not exposed to Au NPs, condition 2: conditioned medium containing 5 nM Ag NPs, condition 3: conditioned medium of cells exposed to Au NPs but not containing NPs; condition 4: conditioned medium of cells exposed to Ag NPs not containing and NPs nor any EVs (EVs removed upon ultracentrifugation). Next, media were removed, cells washed twice with ice-cold PBS, after which they were reseeded in new 24 well plates at a density of $1 * 10^4$ cells/well, containing either the Radius™ 24 well cell migration assay plate (Cell Biolabs Inc, San Diego, CA, USA) or a 8 µm-pore Boyden chamber (Cell Biolabs Inc, San Diego, CA, USA). After 24 h, the gel plug was removed from the Radius migration assay plate, allowing the cells to migrate. For cell invasion studies, cell media were removed and fresh serum-free medium was given to the cells in the upper compartment, while to lower compartment contained full serum-containing medium. Cell migration was measured fluorometrically after 12 h, by fixing the cells, staining with PI (Thermofisher Scientific, USA) and using the imaging shield which only allows light from the original gel plug-covered area to be measured. For cell invasion, the Boyden chamber was removed after 12 h and any cells that had migrated through the pores were counted. This concerns any cells present in the lower compartment (medium or bottom of the well) as well as cells that were scraped off from the bottom side of the Boyden chamber. All cells were collected and counted using a Burker chamber.

**Statistical analysis**

All statistical analyses were performed using GraphPad 9.0 statistical analysis software. To determine significant differences between groups, 2-way ANOVA tests were performed with Tukey post-hoc test, unless otherwise indicated in the corresponding text. The levels of significance and number of independent repeats are indicated with every data point given.

## ASSOCIATED CONTENT

**Supporting Information**. Supporting figures (6) and a supporting table are included as a pdf document accompanying this manuscript and is available free of charge. The supporting figures display (S1) mitochondrial ROS results for the different cell types exposed to the various NPs, (S2) confocal images of the cell lines incubated with fluorescently tagged EVs, (S3) uptake of EVs by B16-F10 cells (S4) a miRNA gene target enrichment network analysis and (S5 and S6) Ag NP-induced immune responses. The supporting table displays the most significantly up- or downregulated miRNAs that were used as input for MIENTURNET analysis.

## AUTHOR INFORMATION


### Corresponding Author

*e-mail: s.soenen@kuleuven.be, Orcid ID: https://orcid.org/0000-0003-2390-3133


### Author Contributions

The manuscript was written through contributions of all authors. All authors have given approval to the final version of the manuscript.

## ACKNOWLEDGMENT


This work has been performed thanks to financial support from KU Leuven BOF funding (C3 3M210428; C2 3M220302).

## Reference list


1. Wolfram J, Ferrari M. Clinical cancer nanomedicine. *Nano Today* 2019;25:85-98. doi:10.1016/j.nantod.2019.02.005.

2. Seleci M, Ag Seleci D, Joncyzk R, Stahl F, Blume C, Scheper T. Smart multifunctional nanoparticles in nanomedicine. *BioNanoMaterials* 2016;17(1-2):33-41. doi:10.1515/bnm-2015-0030.

3. Veiseh O, Kievit FM, Ellenbogen RG, Zhang M. Cancer Cell Invasion: Treatment and Monitoring Opportunities in Nanomedicine. *Adv. Drug Deliv. Rev.* 2011. doi:10.1016/j.addr.2011.01.010.

4. Overchuk M, Zheng G. Overcoming obstacles in the tumor microenvironment: Recent advancements in nanoparticle delivery for cancer theranostics. *Biomaterials* 2018;156:217-237. doi:10.1016/j.biomaterials.2017.10.024.

5. Zhang Y, Elechalawar CK, Hossen MN, et al. Gold nanoparticles inhibit activation of cancer-associated fibroblasts by disrupting communication from tumor and microenvironmental cells. *Bioact. Mater.* 2021;6(2):326-332. doi:10.1016/j.bioactmat.2020.08.009.

6. Sindhwani S, Syed AM, Ngai J, et al. The entry of nanoparticles into solid tumours. *Nat. Mater.* 2020;19(5):566-575. doi:10.1038/s41563-019-0566-2.

7. Yue X, Zhang Q, Dai Z. Near-infrared light-activatable polymeric nanoformulations for combined therapy and imaging of cancer. *Adv. Drug Deliv. Rev.* 2017;115:155-170. doi:10.1016/j.addr.2017.04.007.

8. Dai Q, Wilhelm S, Ding D, et al. Quantifying the Ligand-Coated Nanoparticle Delivery to Cancer Cells in Solid Tumors. *ACS Nano* 2018;12(8):8423-8435. doi:10.1021/acsnano.8b03900.

9. Hansen AE, Petersen AL, Henriksen JR, et al. Positron Emission Tomography Based Elucidation of the Enhanced Permeability and Retention Effect in Dogs with Cancer Using Copper-64 Liposomes. *ACS Nano* 2015;9(7):6985-6995.

10. Bazak R, Houri M, Achy S El, et al. Cancer active targeting by nanoparticles: a comprehensive review of literature. *J. Cancer Res. Clin. Oncol.* 2016;141(5):769-784. doi:10.1007/s00432-014-1767-3.Cancer.

11. Fathi P, Rao L, Chen X. Extracellular vesicle-coated nanoparticles. *View* 2021;2(2):1-9. doi:10.1002/VIW.20200187.

12. Herrmann IK, Wood MJA, Fuhrmann G. Extracellular vesicles as a next-generation drug delivery platform. *Nat. Nanotechnol.* 2021;16(7):748-759. doi:10.1038/s41565-021-00931-2.

13. Van Niel G, D'Angelo G, Raposo G. Shedding light on the cell biology of extracellular vesicles. *Nat. Rev. Mol. Cell Biol.* 2018;19(4):213-228. doi:10.1038/nrm.2017.125.

14. Dixson AC, Dawson TR, Di Vizio D, Weaver AM. Context-specific regulation of extracellular vesicle biogenesis and cargo selection. *Nat. Rev. Mol. Cell Biol.* 2023. doi:10.1038/s41580-023-00576-0.

15. Mathieu M, Martin-Jaular L, Lavieu G, Théry C. Specificities of secretion and uptake of exosomes and other extracellular vesicles for cell-to-cell communication. *Nat. Cell Biol.* 2019;21(1):9-17. doi:10.1038/s41556-018-0250-9.

16. Huang S, Dong M, Chen Q. Tumor-Derived Exosomes and Their Role in Breast Cancer Metastasis. *Int. J. Mol. Sci.* 2022;23(22). doi:10.3390/ijms232213993.

17. O'Brien K, Breyne K, Ughetto S, Laurent LC, Breakefield XO. RNA delivery by extracellular vesicles in mammalian cells and its applications. *Nat. Rev. Mol. Cell Biol.* 2020;21(10):585-606. doi:10.1038/s41580-020-0251-y.

18. Ueta E, Tsutsumi K, Kato H, et al. Extracellular vesicle-shuttled miRNAs as a diagnostic and prognostic biomarker and their potential roles in gallbladder cancer patients. *Sci. Rep.* 2021;11(1):1-13. doi:10.1038/s41598-021-91804-0.

19. Zomer A, Maynard C, Verweij FJ, et al. In vivo imaging reveals extracellular vesicle-mediated phenocopying of metastatic behavior. *Cell* 2015;161(5):1046-1057. doi:10.1016/j.cell.2015.04.042.

20. Lara P, Palma-Florez S, Salas-Huenuleo E, et al. Gold nanoparticle based double-labeling of melanoma extracellular vesicles to determine the specificity of uptake by cells and preferential accumulation in small metastatic lung tumors. *J. Nanobiotechnology* 2020;18(1):1-17. doi:10.1186/s12951-020-0573-0.

21. Park DJ, Yun WS, Kim WC, et al. Improvement of stem cell-derived exosome release efficiency by surface-modified nanoparticles. *J. Nanobiotechnology* 2020;18(1):1-17. doi:10.1186/s12951-020-00739-7.

22. Wu X, Tang T, Wei Y, Cummins KA, Wood DK, Pang HB. Extracellular Vesicles Mediate the Intercellular Exchange of Nanoparticles. *Adv. Sci.* 2022;9(7):1-13. doi:10.1002/advs.202102441.

23. Manshian BB, Pokhrel S, Mädler L, Soenen SJ. The impact of nanoparticle-driven lysosomal alkalinization on cellular functionality. *J. Nanobiotechnology* 2018;16(1):1-13. doi:10.1186/s12951-018-0413-7.

24. Soenen SJ, Rivera-Gil P, Montenegro JM, Parak WJ, De Smedt SC, Braeckmans K. Cellular toxicity of inorganic nanoparticles: Common aspects and guidelines for improved nanotoxicity evaluation. *Nano Today* 2011;6(5):446-465. doi:10.1016/j.nantod.2011.08.001.

25. Peng F, Setyawati MI, Tee JK, et al. Nanoparticles promote in vivo breast cancer cell intravasation and extravasation by inducing endothelial leakiness. *Nat. Nanotechnol.* 2019;14(3):279-286. doi:10.1038/s41565-018-0356-z.

26. Zhu M, Li Y, Shi J, Feng W, Nie G, Zhao Y. Exosomes as extrapulmonary signaling conveyors for nanoparticle-induced systemic immune activation. *Small* 2012;8(3):404-412. doi:10.1002/smll.201101708.

27. Liu LY, Ma XZ, Ouyang B et al. Nanoparticle Uptake in a Spontaneous and Immunocompetent Woodchuck Liver Cancer Model. *ACS Nano* 2020;14(4):4698-4715.

28. Yang W, Wang L, Fang ML, et al. Nanoparticle Surface Engineering with Heparosan Polysaccharide Reduces Serum Protein Adsorption and Enhances Cellular Uptake. *Nano Letters* 2022;22(5):2103-2111.

29. Darvish S, Kahrizi MS, Özbolat G, Khaleghi F, Mortezania Z, Sakhaei D. Silver nanoparticles: biosynthesis and cytotoxic performance against breast cancer MCF-7 and MDA-MB-231 cell lines. *Nanomedicine Res. J.* 2022;7(1):83-92. doi:10.22034/nmrj.2022.01.008.

30. Zhang D, Wu T, Qin X, et al. Intracellularly Generated Immunological Gold Nanoparticles for Combinatorial Photothermal Therapy and Immunotherapy against Tumor. *Nano Lett.* 2019;19(9):6635-6646. doi:10.1021/acs.nanolett.9b02903.

31. Manshian BB, Moyano DF, Corthout N, et al. High-content imaging and gene expression analysis to study cell-nanomaterial interactions: The effect of surface hydrophobicity. *Biomaterials* 2014;35(37):9941-9950. doi:10.1016/j.biomaterials.2014.08.031.

32. Théry C, Witwer KW, Aikawa E, et al. Journal of Extracellular Vesicles Minimal information for studies of extracellular vesicles 2018 (MISEV2018): a position statement of the International Society for Extracellular Vesicles and update of the MISEV2014 guidelines. Available at: https://www.tandfonline.com/loi/zjev20.

33. Mathieu M, Névo N, Jouve M, et al. Specificities of exosome versus small ectosome secretion revealed by live intracellular tracking of CD63 and CD9. *Nat. Commun.* 2021;12(1). doi:10.1038/s41467-021-24384-2.

34. Baietti MF, Zhang Z, Mortier E, et al. Syndecan-syntenin-ALIX regulates the biogenesis of exosomes. *Nat. Cell Biol.* 2012;14(7):677-685. doi:10.1038/ncb2502.

35. Woud WW, van der Pol E, Mul E, et al. An imaging flow cytometry-based methodology for the analysis of single extracellular vesicles in unprocessed human plasma. *Commun.*

*Biol.* 2022;5(1):1-14. doi:10.1038/s42003-022-03569-5.

36. Buzas EI. The roles of extracellular vesicles in the immune system. *Nat. Rev. Immunol.* 2022;23(April). doi:10.1038/s41577-022-00763-8.

37. Muñiz-García A, Romero M, Falcón-Perez JM, Murray P, Zorzano A, Mora S. Hypoxia-induced HIF1α activation regulates small extracellular vesicle release in human embryonic kidney cells. *Sci. Rep.* 2022;12(1):1-14. doi:10.1038/s41598-022-05161-7.

38. Hitomi K, Okada R, Loo TM, Miyata K, Nakamura AJ, Takahashi A. DNA Damage Regulates Senescence-Associated Extracellular Vesicle Release via the Ceramide Pathway to Prevent Excessive Inflammatory Responses. *Int. J. Mol. Sci.* 2020;21(10).

39. Kulshreshtha A, Singh S, Ahmad M, et al. Simvastatin mediates inhibition of exosome synthesis, localization and secretion via multicomponent interventions. *Sci. Rep.* 2019;9(1):1-10. doi:10.1038/s41598-019-52765-7.

40. Shin TH, Ketebo AA, Lee DY, et al. Decrease in membrane fluidity and traction force induced by silica-coated magnetic nanoparticles. *J. Nanobiotechnology* 2021;19(1):1-14. doi:10.1186/s12951-020-00765-5.

41. Marzano M, Bou-Dargham MJ, Cone AS, et al. Biogenesis of Extracellular Vesicles Produced from Human-Stem-Cell-Derived Cortical Spheroids Exposed to Iron Oxides. *ACS Biomater. Sci. Eng.* 2021;7(3):1111-1122. doi:10.1021/acsbiomaterials.0c01286.

42. Chiaradia E, Tancini B, Emiliani C, et al. Extracellular vesicles under oxidative stress conditions: Biological properties and physiological roles. *Cells* 2021;10(7):1-25. doi:10.3390/cells10071763.

43. Murphy DE, de Jong OG, Brouwer M, et al. Extracellular vesicle-based therapeutics: natural versus engineered targeting and trafficking. *Exp. Mol. Med.* 2019;51(3). doi:10.1038/s12276-019-0223-5.

44. Marar C, Starich B, Wirtz D. Extracellular vesicles in immunomodulation and tumor progression. *Nat. Immunol.* 2021;22(5):560-570. doi:10.1038/s41590-021-00899-0.

45. Chen G, Huang AC, Zhang W, et al. Exosomal PD-L1 contributes to immunosuppression and is associated with anti-PD-1 response. *Nature* 2018;560(7718):382-386. doi:10.1038/s41586-018-0392-8.

46. Martini M, De Santis MC, Braccini L, Gulluni F, Hirsch E. PI3K/AKT signaling pathway and cancer: An updated review. *Ann. Med.* 2014;46(6):372-383. doi:10.3109/07853890.2014.912836.

47. Lo HW, Hung MC. Nuclear EGFR signalling network in cancers: Linking EGFR pathway to cell cycle progression, nitric oxide pathway and patient survival. *Br. J. Cancer* 2006;94(2):184-188. doi:10.1038/sj.bjc.6602941.

48. Phan LM, Rezaeian AH. Atm: Main features, signaling pathways, and its diverse roles in dna damage response, tumor suppression, and cancer development. *Genes (Basel)*. 2021;12(6):1-11. doi:10.3390/genes12060845.

49. Rašková M, Lacina L, Kejík Z, et al. The Role of IL-6 in Cancer Cell Invasiveness and Metastasis—Overview and Therapeutic Opportunities. *Cells* 2022;11(22). doi:10.3390/cells11223698.

50. Apte RS, Chen DS, Ferrara N. VEGF in Signaling and Disease: Beyond Discovery and Development. *Cell* 2019;176(6):1248-1264. doi:10.1016/j.cell.2019.01.021.

51. Guo C, You DY, Li H, Tuo XY, Liu ZJ. Spherical silica nanoparticles promote malignant transformation of BEAS-2B cells by stromal cell-derived factor-1α (SDF-1α). *J. Int. Med. Res.* 2019;47(3):1264-1278. doi:10.1177/0300060518814333.

52. He Q, Zhang J, Shi J, et al. The effect of PEGylation of mesoporous silica nanoparticles on nonspecific binding of serum proteins and cellular responses. *Biomaterials* 2010;31(6):1085-1092. doi:10.1016/j.biomaterials.2009.10.046.

53. Sharma U, Pal D, Prasad R. Alkaline phosphatase: An overview. *Indian J. Clin. Biochem.* 2014;29(3):269-278. doi:10.1007/s12291-013-0408-y.

54. Rao SR, Snaith AE, Marino D, et al. Tumour-derived alkaline phosphatase regulates tumour growth, epithelial plasticity and disease-free survival in metastatic prostate cancer. *Br. J. Cancer* 2017;116(2):227-236. doi:10.1038/bjc.2016.402.

55. Leitner BP, Siebel S, Akingbesote ND, Zhang X, Perry RJ. Insulin and cancer: a tangled web. *Biochem. J.* 2022;479(5):583-607. doi:10.1042/BCJ20210134.

56. Tao Y, Pinzi V, Bourhis J, Deutsch E. Mechanisms of Disease: Signaling of the insulin-like growth factor 1 receptor pathway - Therapeutic perspectives in cancer. *Nat. Clin. Pract. Oncol.* 2007;4(10):591-602. doi:10.1038/ncponc0934.

57. Bent EH, Millán-Barea LR, Zhuang I, Goulet DR, Fröse J, Hemann MT. Microenvironmental IL-6 inhibits anti-cancer immune responses generated by cytotoxic chemotherapy. *Nat. Commun.* 2021;12(1):1-13. doi:10.1038/s41467-021-26407-4.

58. Fahrenholtz CD, Swanner J, Ramirez-Perez M, Singh RN. Heterogeneous Responses of Ovarian Cancer Cells to Silver Nanoparticles as a Single Agent and in Combination with Cisplatin. *J. Nanomater.* 2017;2017. doi:10.1155/2017/5107485.

59. Lee S, Rauch J, Kolch W. Targeting MAPK signaling in cancer: Mechanisms of drug resistance and sensitivity. *Int. J. Mol. Sci.* 2020;21(3):1-29. doi:10.3390/ijms21031102.

60. Mittal V. Epithelial Mesenchymal Transition in Tumor Metastasis. *Annu. Rev. Pathol. Mech. Dis.* 2018;13:395-412. doi:10.1146/annurev-pathol-020117-043854.

61. Meulmeester E, Ten Dijke P. The dynamic roles of TGF-β in cancer. *J. Pathol.* 2011;223(2):206-219. doi:10.1002/path.2785.

62. Derynck R, Turley SJ, Akhurst RJ. TGFβ biology in cancer progression and immunotherapy. *Nat. Rev. Clin. Oncol.* 2021;18(1):9-34. doi:10.1038/s41571-020-0403-1.

63. Xu J, Lamouille S, Derynck R. TGF-B-induced epithelial to mesenchymal transition. *Cell Res.* 2009;19(2):156-172. doi:10.1038/cr.2009.5.

64. Ali MRK, Wu Y, Ghosh D, et al. Correction: Nuclear Membrane-Targeted Gold Nanoparticles Inhibit Cancer Cell Migration and Invasion (ACS Nano (2017) 11:4 (3716-3726) DOI: 10.1021/acsnano.6b08345). *ACS Nano* 2020;14(9):12260. doi:10.1021/acsnano.0c07219.

65. Zhang Y, Xiao H, Xiong R, Huang C. Xylan-based ratiometric fluorescence carbon dots composite with delignified wood for highly efficient water purification and photothermal conversion. *Separation and Purification Technology* 2023;324:124513.

66. Ninan N, Goswami N, Vasilev K. The impact of engineered silver nanomaterials on the immune system. *Nanomaterials* 2020;10(5):1-27. doi:10.3390/nano10050967.

67. Fraser JA, Kemp S, Young L, et al. Silver nanoparticles promote the emergence of heterogeneic human neutrophil sub-populations. *Sci. Rep.* 2018;8(1):1-14. doi:10.1038/s41598-018-25854-2.

68. Izci M, Maksoudian C, Gonçalves F, et al. Gold nanoparticle delivery to solid tumors: a multiparametric study on particle size and the tumor microenvironment. *J. Nanobiotechnology* 2022;20(1):1-20. doi:10.1186/s12951-022-01727-9.

69. Solé C, Lawrie CH. MicroRNAs and metastasis. *Cancers (Basel).* 2020;12(1):1-21. doi:10.3390/cancers12010096.

70. Licursi V, Conte F, Fiscon G, Paci P. MIENTURNET: an interactive web tool for microRNA-target enrichment and network-based analysis. *BMC Bioinformatics* 2019;20:545.

## Graphic abstract